

# Evaluating common QTAIM and NCI interpretations of the electron density concentration through IQA interaction energies and 1D cross-sections of the electron and deformation density distributions

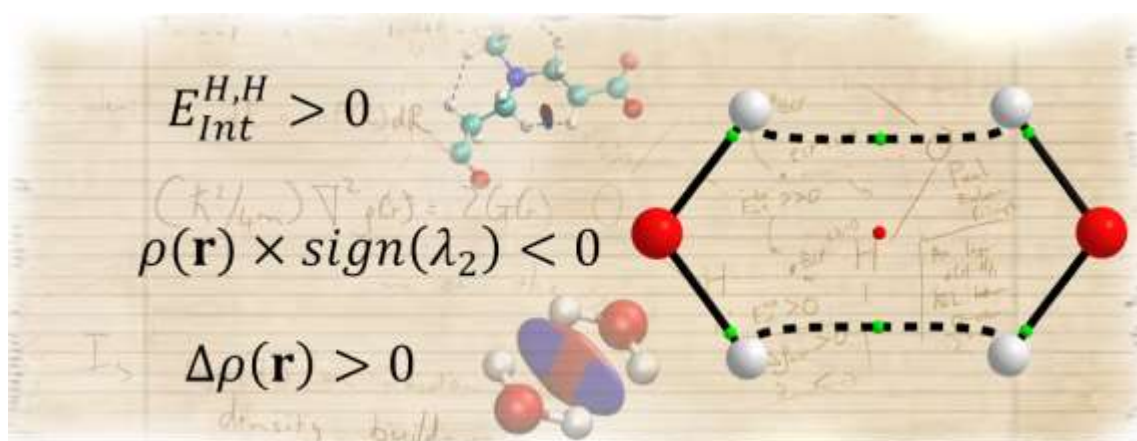
*Ignacy Cukrowski, Jurgens H. de Lange, Adedapo S. Adeyinka, Paidamwoyo Mangondo*

Department of Chemistry, Faculty of Natural and Agricultural Sciences, University of Pretoria, Lynnwood Road, Hatfield, Pretoria 0002, South Africa

## Highlights

- Classical steric clashes might have the same topological features as bonding interactions.
- An AIL can be observed for highly attractive or repulsive interactions.
- An AIL might be a result of either an inflow or outflow of density.
- Locally accumulated density does not imply an attractive interaction or an inflow of density.
- Nature of an interaction can change with molecular environment.

## Graphical abstract



## Abstract

Nine kinds of inter- and intramolecular interactions were investigated by exploring the topology of electron density in the interatomic regions using standard protocols of QTAIM, IQA and NCI techniques as well as in-house developed cross-sections of the electron and deformation density distributions. The first four methods provide the properties of the resultant density distribution in a molecular system whereas the later illustrates the process, inflow or outflow of density from fragments to the interatomic region of an interaction on its formation in a molecular system. We used (i) the QTAIM-defined atomic interaction line, AIL (presence or absence), (ii) IQA-defined interaction energy,  $E_{\text{int}}^{\text{A,B}}$ , and its components, classical  $V_{\text{cl}}^{\text{A,B}}$  and exchange-correlation  $V_{\text{xc}}^{\text{A,B}}$  term, (iii) NCI-defined isosurfaces to identify local regions of accumulated ( $\lambda_2 < 0$ ) or depleted ( $\lambda_2 > 0$ ) density relative to immediate environment, and (iv) deformation density for which  $\Delta\rho(\mathbf{r}) > 0$  indicates an inflow or otherwise an outflow of density on the interaction formation to explore the nature of the interactions. We found (i) AILs for highly attractive and repulsive interactions, regardless whether an inflow ( $\Delta\rho(\mathbf{r}) > 0$ ) or outflow of density into the interatomic region, (ii) no correlation between the signs of  $\lambda_2$  and  $E_{\text{int}}^{\text{A,B}}$ ; both, highly repulsive and attractive, interactions might have locally depleted density and *vice versa*, (iii) locally accumulated density ( $\lambda_2 < 0$ ) does not imply that this is the result of an inflow ( $\Delta\rho(\mathbf{r}) > 0$ ) of density and this equally applies to attractive and repulsive interactions either with or without an AIL. Results obtained demonstrate that the molecular environment can change the character of an interaction radically, from (i) attractive to repulsive, (ii)  $\lambda_2 < 0$  to  $\lambda_2 > 0$ , or (iii)  $\Delta\rho(\mathbf{r}) > 0$  to  $\Delta\rho(\mathbf{r}) < 0$ ; hence, none of the topological indices used here, either separately or combined, can be used to definitely predict the (de)stabilizing nature of an interaction except highly repulsive ones for which the absence of AIL, interatomic density depletion and outflow of density on interaction formation are observed.

Keywords: QTAIM; IQA; NCI; deformation density; chemical bonding; atomic interaction line; bond path.

## 1. Introduction

The analysis of the topology of the electron density, for instance as it is used in the Quantum Theory of Atoms in Molecules (QTAIM) [1] and the more recent Non-Covalent Interactions (NCI) [2–4] method, is commonly used to identify and classify inter- and intramolecular interactions in molecular systems. Due to the relatively low computational costs, these methods (under the umbrella of Quantum Chemical Topology (QCT) [5]) have found widespread use in all fields of chemistry, ranging from drug-design [6] to catalysis [7] to large biological systems [8]. In QTAIM, the presence of a bridge of maximal electron density between two atoms, commonly referred to as a bond path or an atomic interaction line (AIL), is observed for most cases where a classical chemist would expect a chemical bond. Consequently, many chemists commonly use the presence of an AIL as an indication of a chemical bond [9–12] or, at the very least, a bonding interaction [13,14]. Numerous cases exist, however, where either (i) classical chemists expect a bonding interaction (or it is shown through other methods, such as energy decomposition schemes) but no AIL is present [15], or (ii) steric repulsion is believed to exist, but an AIL is seen regardless [16–26]. These problem cases have resulted in a very long debate, questioning on one hand the validity and interpretation of QTAIM results [27–31] and on the other hand the nature of classical chemical concepts, such as steric repulsion [32–36]. The chemical bond itself also came into question since, as Bader put it, ‘*Why should a bond path, which recovers all Lewis structures, not be associated with bonding in other cases?*’ [28]. Although many regard the debate to be stale [37, 38], new papers are still being published regarding the interpretation and physical nature of AILs [39–46].

NCI managed to solve one branch of QTAIM-associated problems, by showing that the absence of an AIL does not imply that electron density cannot be concentrated in the bonding region of an interaction. NCI identifies inter- and intramolecular interactions by finding regions of low electron density between atoms where the reduced density gradient (RDG) tends to zero [2]. These regions are then classified as either “stabilizing”, when electron density is concentrated, or “destabilizing”, when electron density is depleted [2–4,47,48]. NCI therefore supplements typical QTAIM analysis in three ways: (i) it identifies an interaction in 3D space, whereas QTAIM only shows bridges, (ii) it can detect electron density concentration, despite the absence of an AIL, and (iii) it can also identify interactions due to regions of electron depletion. NCI can also be used to approximately analyse interactions based only on the geometries (without the need for an electronic structure calculation) thereby allowing it to be used for very large systems. However, NCI will always show a region of concentration wherever an AIL is present [49], and is thus marred by the same problem of interpretation with regards to controversial interactions (such as the CH•••HC interactions in the

bay of biphenyl). Both NCI and QTAIM are very attractive tools for a computational chemist to use, for their relative simplicity, insight and low computational cost but interpreting the results of these methods, especially in the realm of potentially new and not-yet-understood interactions, is still very unclear.

The so-called orthodox interpretation of an AIL, as given by Bader [50], is that it signals a *bonding interaction*, and only at equilibrium geometries (when no net forces are acting on the atoms) it can be related to a chemical bond. Bader arrived [50] to this statement by first pointing out that the sign of the eigenvalues  $\lambda_1$ ,  $\lambda_2$  and  $\lambda_3$ , of the Hessian matrix (the ordered matrix of second derivatives in 3D space), as well as the sum of eigenvalues, the Laplacian ( $\nabla^2\rho(\mathbf{r})$ ), can be related to the concentration or depletion of electron density in a specific axis or at a point, respectively. Specifically, when  $\nabla^2\rho(\mathbf{r}) > 0$ , the second-order change in the electron density is positive at  $\mathbf{r}$ , the density at  $\mathbf{r}$  is less than the average of its surrounding density, and the electron density is said to be *depleted*; similarly, electron density is *concentrated* at  $\mathbf{r}$  when  $\nabla^2\rho(\mathbf{r}) < 0$ . The same applies to the individual component eigenvalues of the Hessian matrix, but along a specific axis. The topological condition for an AIL to be present is that density is depleted *along* the AIL ( $\lambda_1 > 0$ ), but concentrated across it ( $\lambda_2$  and  $\lambda_3 < 0$ ). By convention,  $\lambda_1 \geq \lambda_2 \geq \lambda_3$ , and  $\lambda_1 > 0$  between any two atoms, hence  $\lambda_2$  is of particular importance because its sign will determine whether electron density is concentrated or depleted across an interaction; this is also the base of classification used by NCI. Bader then linked [1,50] the concentration of density (as measured by the second-derivative of the electron density) through the local statement of the virial theorem, to a concept of bonding: that a “build-up” of charge is observed in the bonding region upon formation of a chemical bond [51–55]. Through this reasoning Bader then suggested that a concentration and depletion of electron density is stabilizing and destabilizing, respectively, and therefore that the presence of an AIL (a maximal concentration of density) can be regarded as a bonding interaction. The same interpretation was then applied in NCI, with regions of concentration deemed as stabilizing and attractive, and regions of depletion often referred to as steric strain [2,47–49].

While there have been debates with regards to the nature of the energetic stabilization which occurs upon bond formation (whether it is potential [1,51,52] or kinetic in origin [56,57]), there can be little doubt that one of the key features of any form of chemical bonding is increased charge density in the bonding region. This is true even for atoms bound only by dispersion, where, as Feynman [53] puts it, “*each atom is attracted to the distortion, centred in the bonding region, of its own charge density*”, as well as very electrostatic or ionic interactions, where the increased density is mainly localized to one atom (but still more so within the bonding region). However, it is not

clear how this “build-up” of charge can be measured. Is the concentration or depletion of density, as used by the orthodox interpretation of an AIL or NCI regions of interactions, truly indicative of increased or decreased electron density in the bonding region, respectively, and thus synonymous with energetic stabilization or destabilization? Is it a measure of the electron density of a small region relative only to its environment, or can it be linked with the electron density relative to an unbound state? Finally, Pendás et al [38] have provided an alternative interpretation of an AIL, which suggests that an AIL signals a privileged exchange-correlation channel. Their interpretation provides an elegant alternative to the orthodox QTAIM interpretation of AILs as bonding interactions. Their interpretation has been put to the test by Tognetti and Joubert [58] who measured the QTAIM-defined delocalization indices as well as the exchange-correlation contribution to the IQA-defined diatomic interaction energy between competing (close) pairs of atoms, and found that Pendás’ interpretation holds with a small margin of ambiguity.

In this work we will investigate Bader’s claim, as it is commonly used in QTAIM and NCI literature, by careful investigation of the electron density and its changes in a wide range of interactions in various molecular systems, ranging from equilibrium to non-equilibrium geometries, as well as several controversial CH•••HC interactions in different environments. QTAIM and NCI analyses, as well as the changes observed with changing geometries and environments, will be compared with results from the Interacting Quantum Atoms [59,60] (IQA) energy decomposition technique, as well as investigated carefully with one dimensional cross-sections of the electron density. We also investigate the use of the deformation density as an alternative measure of the “build-up” of charge in the bonding region.

## 2. Methods and Computational Details

All geometry optimizations and electronic structure calculations were performed in Gaussian 09, revision D [61] at the RMP2/6-311++G(d,p) level of theory in solvent (PCM/UFF) except water dimer where RMP2/6-31+G(d,p) in the gas phase was used. QTAIM and IQA analyses were carried out in AIMAll [62] using the Proaim integration algorithm with very high angular quadrature outside the beta sphere for IQA calculations. NCI calculations were carried out using NCIPLOT 2.0 [4] and corresponding isosurfaces were visualized in VMD 1.9.1 [63]. Finally, one-dimensional cross-sections of the electron and deformation densities along  $\lambda_2$  eigenvectors were performed using in-house software.

In order to calculate the cross-sections of the electron and deformation densities, the geometric interaction point (GIP) was determined which corresponds to the point of lowest density directly

between two nuclei. The eigenvector corresponding to the  $\lambda_2$  eigenvalue of the Hessian matrix was then calculated, and two new coordinates were generated at a specific distance (usually 0.05 au) in both directions along this vector. The electron densities were then recorded at these points and new coordinates generated based on the eigenvectors corresponding to the  $\lambda_2$  eigenvalues at these points. This process was repeated until a pre-determined length (usually 2 Å in both directions) was reached. For brevity, the entire path followed through this process is referred to the  $\lambda_2$ -eigenvector. The  $\lambda_2$ -eigenvector therefore will always originate from the GIP (which occasionally may coincide with a QTAIM-defined bond critical point, BCP) and will pass through any corresponding NCI-defined interaction critical point (ICP) or BCP, ring critical point (RCP) and cage critical point (CCP). However, in congested molecules the  $\lambda_2$ -eigenvector corresponds to the cross-sections of multiple interactions and in such cases the path followed for the cross-section was calculated as a straight line along the initial  $\lambda_2$ -eigenvector at the GIP. In order to calculate the cross-sections of the deformation density, the electron density for each fragment was calculated along the same  $\lambda_2$ -eigenvector as for the cross-section of the molecular electron density. The cross-section of the molecular density was then subtracted from the sum of fragment densities to give the cross-section of the deformation density.

To generate a wide range of structures for water dimers in four different conformations, selected interatomic distances in each conformer were fixed at preselected values and the structures were optimized with geometrical constraints shown in Table S1 of the SI. The deformation density was generated from single point calculations (SPCs) carried out on each monomer.

Two conformers of (un)protonated 2,2'-bipyridine were generated by keeping the N,C,C,N dihedral angle (DA) fixed at  $DA(N,C,C,N) = 0^\circ$  and  $180^\circ$ , corresponding to *s-cis* and *s-trans* forms, respectively. Deformation densities were calculated by fragmenting each structure into two radical pyridine fragments and carrying out SPCs at UMP2 level with duplet multiplicities, as shown in Figure S1 of the SI.

A conformational analysis of nitrilotri-3-propionic acid (NTPA) was carried out using Spartan '10 [64] and the MMFFaq force field. Deformation densities were obtained from SPCs carried out on four radical fragments, three duplet  $\bullet(\text{CH}_2)_2\text{COO}^-$  and one quartet N-tom fragment as shown in Figure S2 of the SI.

Deformation densities of monoprotonated aliphatic polyamine, triethylaminetetramine (2,2,2-tet) were calculated by fragmenting each conformer into three radical fragments (corresponding to two

duplet fragments,  $\bullet(\text{CH}_2)_2(\text{NH}_3)$  and  $\bullet(\text{CH}_2)_2(\text{NH}_2)$ , and a triplet  $\bullet(\text{NH})(\text{CH}_2)_2(\text{NH})\bullet$  fragment, as shown in Figure S3 of the SI.

Cross-sections of the electron and deformation densities of selected interactions were calculated along the  $\lambda_2$ -eigenvector at the GIP except water dimers for which BCP was used to generate the initial value of the eigenvector.

### 3. Results and Discussion

#### 3.1 Water dimers

Figure 1 shows four water dimers, **d1** to **d4**, where water molecules were arranged in various relative configurations to test different competing intermolecular interactions. Dimer **d1** represents the lowest energy equilibrium structure, with the molecules bonded with a classical intermolecular O–H hydrogen bond. The remaining dimers were selected with the aim to simulate intermolecular interactions in a crowded (strained) environment: (i) dimer **d2** was prepared to test an O $\cdots$ O interaction, with hydrogens (and oxygen lone-pairs) arranged in a perpendicular manner, (ii) dimer **d3** was constructed to study the competition between O $\cdots$ H and O $\cdots$ O interactions in the same space, with water molecules approaching in the plane, and (iv) in dimer **d4**, the head-on approach of hydrogens in a planar arrangement allowed for studying H $\cdots$ H interactions. In each dimer, the distance of the primary interaction was varied:  $d(\text{H5}\cdots\text{O1})$  in **d1**,  $d(\text{O1}\cdots\text{O4})$  in **d2** and **d3**, and  $d(\text{H2}\cdots\text{H4}) = d(\text{H5}\cdots\text{H6})$  in **d4**.

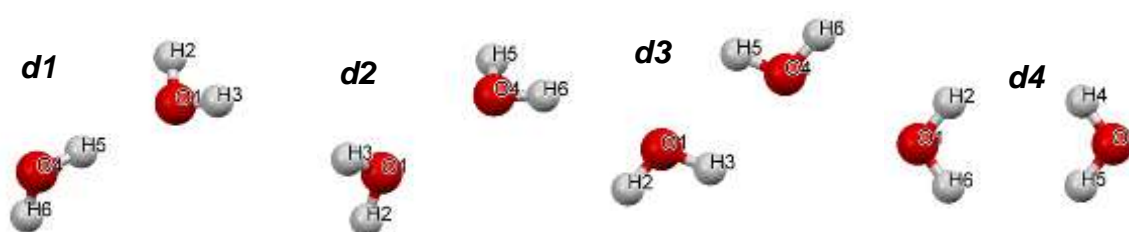


**Figure 1.** Ball-and-stick representation of water dimers considered in this work.

**Energy Profiles and Molecular Graphs.** The electronic energy of dimer **d1** exhibits a global minimum at  $d(\text{O}\cdots\text{H}) = 1.946 \text{ \AA}$  but the electronic energy of dimers **d2**, **d3** and **d4** (as shown in Figure 2) continuously increases as  $d(\text{A}\cdots\text{B})$  decreases, demonstrating that these dimers are truly in unfavourable conformations (with constraints removed in the optimization operations, dimers **d2-d4** revert to the **d1** configuration). The variation in QTAIM-defined molecular structures is also

shown in Figure 2. AILs are found for the O•••H and O•••O interactions in *d1* and *d2*, respectively. Whilst the AIL between O1 and H5 in *d1* is entirely expected and easily interpreted as a classical (stabilizing) H-bond, the interaction between O1 and O4 in *d2* is clearly destabilizing the dimer, hence the significance of the AIL between these atoms is difficult to interpret. It is important to note that the general feature of topology of the electron density between A and B in *d1* as well as in *d2* remains essentially the same at all  $d(A\text{--}B)$  distances – a single AIL is always observed. A different picture is observed for *d3* where initially a single and straight AIL is seen at  $d(\text{O--O}) < \sim 2.4 \text{ \AA}$ , which splits into two AILs at  $d(\text{O--O}) \sim 2.4 \text{ \AA}$  and as a result two BCPs and a RCP are present.

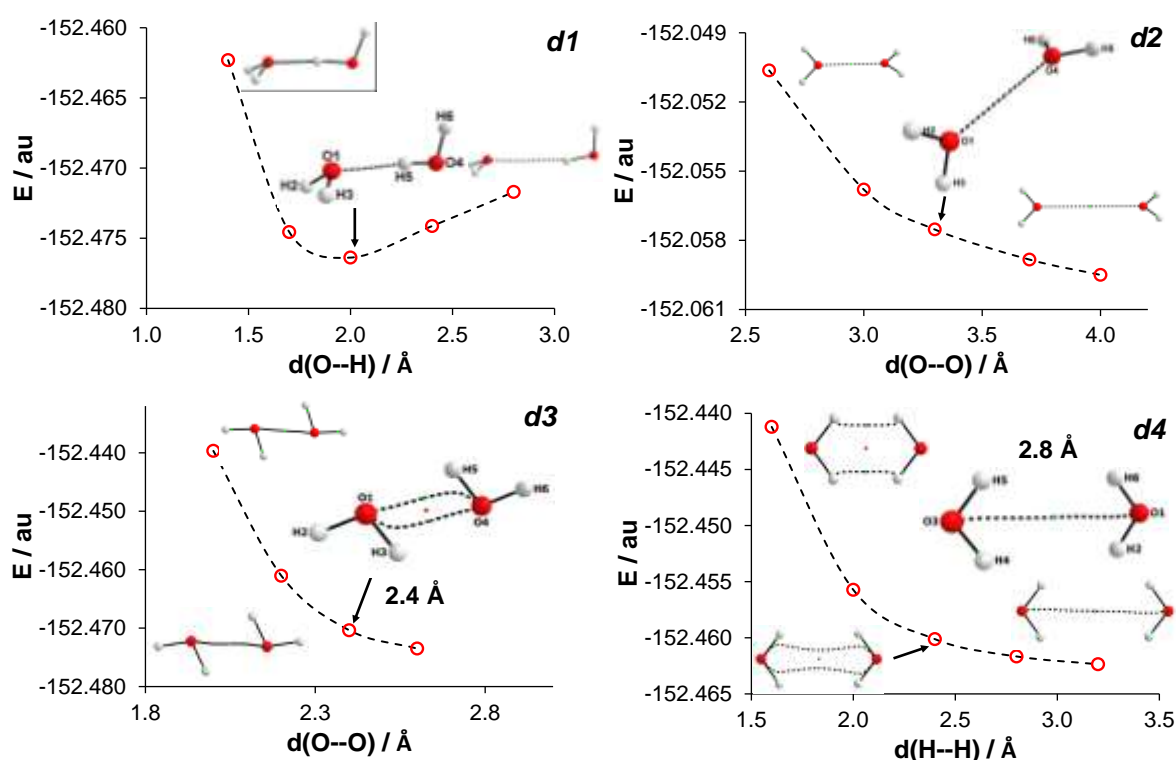


**Figure 2.** Variation in  $E$  with interatomic distance for the indicated water dimers also showing representative molecular graphs.

However, regardless of the interatomic distance, AILs are always linking oxygen atoms. Finally, in *d4*, AILs are initially observed for the H•••H interactions at  $d(\text{H--H}) \leq \sim 2.0 \text{ \AA}$ , with a RCP between oxygen atoms in the middle of the intermolecular six-membered ring. At distances larger than about  $2.0 \text{ \AA}$ , AILs are rather seen between oxygen atoms; initially, at  $d(\text{H--H}) \sim 2.4 \text{ \AA}$  a bifurcated AIL (including RCP) is observed which changes to a single AIL at  $d(\text{H--H}) \geq 2.8 \text{ \AA}$ .



It is fairly clear from Figure 2 that the presence of AILs and their interpretation is not quite obvious. This is because (i) AILs seem to appear between atoms involved in both, classically attractive and repulsive, interactions and (ii) in the case of *d3* and *d4*, the change in the molecular graphs does not seem to correlate with any significant change in the electronic energy which decreases monotonically throughout. Also, the appearance of bifurcated AILs in *d3* and *d4* cannot be easily explained, although (following Bader [1]) they might be examples of “catastrophe points” signalling unstable metafolds. The traditional interpretation of Bader, which states that AILs signify “bonding” interactions [50], is difficult to apply to most of these interactions; it is only for the equilibrium structure of *d1* where the AIL can be truly interpreted as resembling a chemical bond. We therefore turn to NCI for additional insight.

**NCI analysis.** The NCI regions of interaction (colour-coded blue for  $\lambda_2 < 0$  and red for  $\lambda_2 > 0$ ) for each water dimer at selected  $d(\text{A--B})$  values are shown in Figure 3; for a full set of NCI plots see Figures S4 to S7 in the SI. Superficially, NCI correlates well with the molecular graphs: an AIL is seen when  $\lambda_2 < 0$  and the density is said to be concentrated (in the QTAIM and NCI terminology). This is not surprising and has been pointed out before [50]. The spatial property of NCI-regions expands the analysis and is of great help in monitoring variation in the electron density distributions throughout a molecular system. For instance, in *d3* at  $d(\text{O--O}) = 2.4 \text{ \AA}$ , a very small region is seen directly between O-atoms where  $\lambda_2 > 0$ , whereas large regions, with  $\lambda_2 < 0$ , are seen between the  $\text{H}\cdots\text{O}$  interactions. This observation clearly shows that, even though the AIL always links O-atoms for all  $d(\text{O--O})$  in *d3*, AIL might be influenced by the  $\lambda_2 < 0$  regions involving the  $\text{H}\cdots\text{O}$  interactions which, in turn, can give rise to features such as bent AILs as well as splitting at

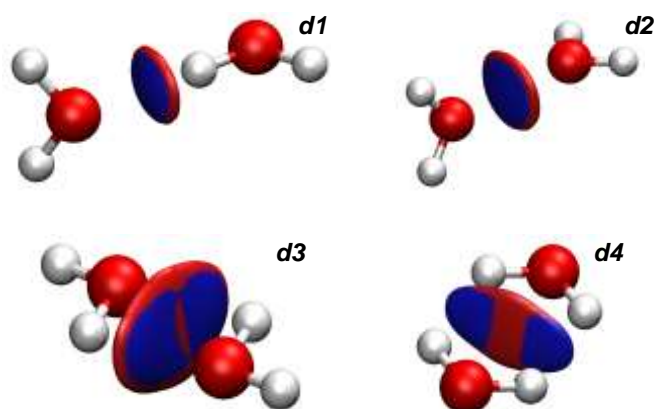


**Figure 3.** NCI isosurfaces (with RDG isovalue = 0.9 au) for water dimers: *d1*)  $d(\text{O--H}) = 2.0 \text{ \AA}$ ; *d2*)  $d(\text{O--O}) = 1.6 \text{ \AA}$ ; *d3*)  $d(\text{O--O}) = 2.4 \text{ \AA}$ ; *d4*)  $d(\text{H--H}) = 2.0 \text{ \AA}$ . Isosurfaces are coloured from blue to red by  $-0.03 \leq \rho(r) \times \text{sign}(\lambda_2) \leq +0.03$  au.

$d(\text{O}\cdots\text{O}) = 2.4 \text{ \AA}$  (see Figure 2c). Furthermore, regions where  $\lambda_2 < 0$  are seen for the  $\text{H}\cdots\text{H}$  interactions, with a clear region of  $\lambda_2 > 0$  for the  $\text{O}\cdots\text{O}$  interaction in **d4** and in this case it correlates with the presence of AILs linking H-atoms at short distances. However, as  $d(\text{H}\cdots\text{H})$  increases, the region where  $\lambda_2 > 0$  vanishes and is replaced by a homogeneous  $\lambda_2 < 0$  region, which is spread out between the  $\text{H}\cdots\text{H}$  and  $\text{O}\cdots\text{O}$  interactions as shown in Figure S7 of the SI.

A clear interpretation of NCI-defined isosurfaces in terms of bonding interactions might be confusing because regions where (i)  $\lambda_2 < 0$  have been described as “concentrating”, “stabilizing” or “attractive”, whereas (ii)  $\lambda_2 > 0$  are referred to as “depletion”, “strain” or “destabilization” [2–4,47–49]. It appears that, in the NCI interpretations, the locally increased density became synonymous with attractive and stabilizing interaction (opposite interpretation applies to  $\lambda_2 > 0$ ). Using these interpretations, however, one would have to attribute both the  $\text{O}\cdots\text{H}$  (in **d1**) and  $\text{O}\cdots\text{O}$  (e.g., in **d2**), as “attractive” interactions. Hence, it is reasonable to question whether it is correct to state that a concentration of density (implying  $\lambda_2 < 0$ ) is indeed *attractive* or *stabilizing* and to gain further insight we now turn to the IQA method.

**IQA Analysis.** Table 1 shows the interaction energies,  $E_{\text{int}}^{\text{A,B}}$ , as well as its components, the electrostatic term  $V_{\text{cl}}^{\text{A,B}}$  and exchange-correlation term,  $V_{\text{xc}}^{\text{A,B}}$ . A few interesting patterns are observed within the IQA analysis of the water dimers: (i) all  $\text{O}\cdots\text{H}$  interactions, especially the AIL-linked  $\text{O1}\cdots\text{H5}$  interaction in **d1**, are highly attractive ( $E_{\text{int}}^{\text{A,B}} < 0$ ) and electrostatic in nature ( $|V_{\text{cl}}^{\text{A,B}}| \gg |V_{\text{xc}}^{\text{A,B}}|$ ), (ii) all  $\text{O}\cdots\text{O}$  and  $\text{H}\cdots\text{H}$  interactions are repulsive and (iii) except for the  $\text{O}\cdots\text{H}$  interactions in **d1** and **d3**, IQA and NCI results do not correlate. The last observation shows that when  $\lambda_2 < 0$  in the bonding region of an interaction, it does not necessarily result in the two atoms being physically attracted towards each other. To support this, let us consider interactions in **d4** as an example. At  $d(\text{H}\cdots\text{H}) = 1.6 \text{ \AA}$ , IQA shows a repulsion of +62.0 kcal/mol between each hydrogen pair, despite  $\lambda_2 = -0.0210 \text{ au}$ . On the other hand, one observes  $\lambda_2 = 0.0176 \text{ au}$  in the bonding region for the  $\text{O}\cdots\text{O}$  interaction and this correlates well with a large repulsion of +166.9 kcal/mol at  $d(\text{H}\cdots\text{H}) = 1.6 \text{ \AA}$  as well as with a common perception of steric hindrance even though O-atoms are not involved in a direct contact. However, at  $d(\text{H}\cdots\text{H}) = 2.8 \text{ \AA}$ , the large repulsion between oxygens is still present (+126.7 kcal/mol) but now we observe  $\lambda_2 < 0$  in the bonding region as well as an AIL.

The interpretation that AILs and NCI regions of density concentration are stabilizing in nature [1,2,50] rests upon the concept that an increase in charge density in the bonding region of an interaction is associated with typical bonding mechanisms. Hence, the sign of  $\lambda_2$  gives an

indication of bonding interactions for the most commonly accepted chemical bonds, such as the O•••H interaction in **d1**. However, since the sign of  $\lambda_2$  gives strictly the local density increase (or decrease) *relative* to adjacent density regions, one might wonder whether its interpretation in terms of attractive (or stabilizing) contribution is equally applicable for all interactions. Specifically, in highly congested systems (such as the **d3** and **d4** water dimers) or isolated interactions in non-equilibrium geometries (such as the O•••O interaction in the **d2** water dimer) the use of the sign of  $\lambda_2$  only shows a local maximum, minimum (or inflection point) of electron density, but does not give any indication of an *increase* due to an inflow (or *decrease* caused by an outflow) in the density upon the formation of an interaction.

**Table 1.** Analysis of interactions in water dimers, **d1-d4**, in terms of interaction energies and electron density in the interatomic bonding region.

Dimer	Distance Å	Interaction A•••B	$E_{\text{int}}^{\text{A,B}}$ <sup>a</sup>	$V_{\text{cl}}^{\text{A,B}}$ <sup>a</sup>	$V_{\text{XC}}^{\text{A,B}}$ <sup>a</sup>	AIL	$\rho(r) \times \text{sign}(\lambda_2)$ <sup>b</sup>	$\Delta\rho(r)_{\text{GIP}}$ <sup>c</sup>
<i>d1</i>	1.946	O1•••H5	-126.1	-116.3	-9.8	Yes	-0.0240	+0.0010
		O1•••O4	158.4	163.3	-4.9	No	-	-
<i>d2</i>	2.6	O1•••O4	157.2	168.6	-11.4	Yes	-0.0178	-0.0036
		O1•••H5	-76.2	-76.1	-0.1	No	-	-
<i>d3</i>	2.0	O1•••O4	154.1	191.0	-36.9	Yes	-0.0524	-0.0094
		O1•••H5	-121.3	-117.3	-4.0	No	-0.0406	-0.0069
<i>d4</i>	1.6	H5•••H6	62.0	64.7	-2.6	Yes	-0.0210	+0.0007
		O1•••O3	166.9	175.5	-8.6	No	+0.0176	-0.0015
		O1•••H5	-103.0	-100.3	-2.7	No	-0.0233	-0.0001
		H5•••H6	45.2	45.5	-0.5	No	-0.0032	+0.0002
	2.4	O1•••O3	140.0	141.8	-1.8	Yes <sup>d</sup>	+0.0037	+0.0001
		O1•••H5	-78.7	-78.2	-0.4	No	-0.0036	+0.0002
		H5•••H6	39.6	39.7	-0.2	No	-0.0013	+0.0001
		O1•••O3	126.7	127.6	-0.8	Yes	-0.0016	+0.0001
2.8	H5•••H6	39.6	39.7	-0.2	No	-0.0013	+0.0001	
	O1•••O3	126.7	127.6	-0.8	Yes	-0.0016	+0.0001	
		O1•••H5	-70.0	-69.7	-0.1	No	-0.0015	+0.0001

<sup>a</sup>Diatomic interaction energies and decomposed components, all in kcal/mol; <sup>b</sup>Values in au at GIP; <sup>c</sup>The deformation density in au at GIP; <sup>d</sup>The AIL is bifurcated into two O•••O AILs, with 2 BCPs and a RCP.

Hence, we decided to investigate two aspects of the density distribution with closer focus on: (i) the *resultant* distribution of density at a specific state or geometry of a molecular system and (ii) the *processes* which transform the density from the initial (non-interacting fragments) to final topology of molecular state under consideration. Within this framework, a *resultant* electron concentration shows where the electron density is at a local maximum, whereas the *processes* at work show how

the density contribution came to be. In order to study these phenomena, we report here the 1D density cross-sections of specific interactions in the water dimers, as well as the 1D cross-sections of the deformation density of each dimer, using water monomers as initial constructor states, according to the methodology set out in Section 2.

**Density cross section and deformation density analysis.** Figure 4(a) shows the density cross-sections of the O•••H and O•••O interactions in *d1* and *d2*. Remarkably, there is no qualitative difference between the density cross-sections perpendicular to the A--B axis of the *d1* and *d2* dimers: a local maximum is seen directly between atoms involved. Because of that, the observed topology generates a point in space where the first order change crosses zero, resulting in a bond critical point, and a region where the second-order change is negative, as shown in Figure S8 of the SI. Furthermore, an almost identical variation obtained for the first and second order changes in *d1* and *d2* indicates that the *resultant* electron density distribution is qualitatively identical for these two radically different interactions. However, the deformation density ( $\Delta\rho(r)$ ) cross-sections,

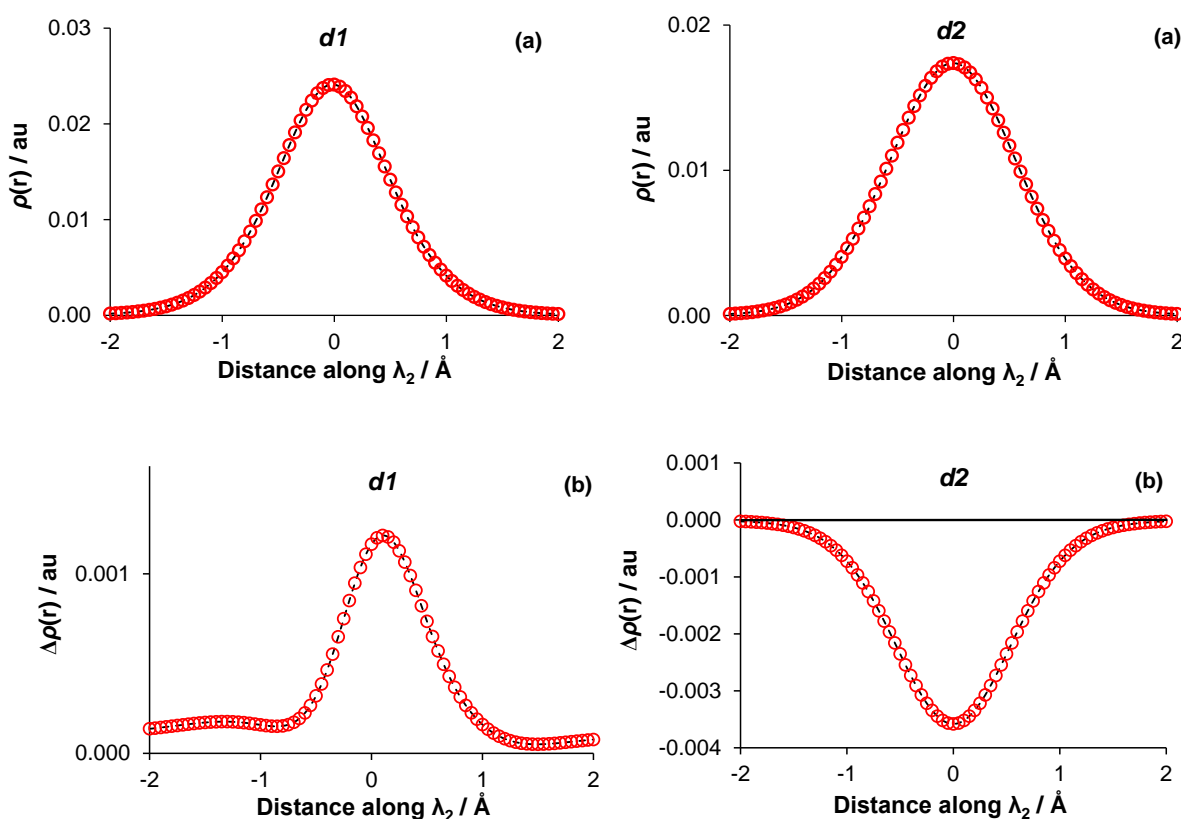


**Figure 4.** Cross section of (a) the electron density and (b) the deformation density along  $\lambda_2$  eigenvector for *d1* at  $d(\text{O--H}) = 1.946 \text{ \AA}$  and *d2* at  $d(\text{O--O}) = 2.6 \text{ \AA}$ . The origin of the cross-sections for *d1* and *d2* are the BCP(O1,H5) and BCP(O1,O4), respectively.

shown in Figure 4b, uncover the different nature of these two interactions. In **d1**, forming the O•••H interaction resulted in  $\Delta\rho(\mathbf{r}) > 0$  with an inflow of electron density into the bonding region which is consistent with the concept of chemical bonding. On the other hand, forming the O•••O interaction in **d2** resulted in a negative deformation density. This appears to correlate well with the repulsive nature of this interaction for which it is favourable for electron density to be removed (*dissipated*) from the bonding region of the O•••O interaction. The deformation density thus shows two very different processes which give rise to similar final density distributions.

The understanding and interpretation of NCI plots, as well as molecular graphs, for dimers **d3** and **d4** is facilitated greatly by cross-sections of the electron density shown for **d4** in Figure 5 and for **d3** in Figure S9 in the SI. At short  $d(\text{H--H})$ , *e.g.*, 1.6 Å, the cross-section of the electron density in **d4** shows two clear peaks, corresponding to the BCPs between hydrogen atoms, and a local minimum, corresponding to the RCP between oxygen atoms. As  $d(\text{H--H})$  gradually increases, the density at BCPs corresponding to the H•••H interactions shows a faster decline than density attributed to the RCP of the O•••O interaction. Finally, at  $d(\text{H--H}) \geq 2.8$  Å, a single local maximum is observed which corresponds to the BCP of the O•••O interaction. The patterns observed in the first- and second-order changes in the electron distribution of **d4** show very much what one would expect from the above analysis: the first order change crosses the X-axis three times at short  $d(\text{H--H})$ , corresponding to two BCPs and a RCP, and the second order change shows clear regions of concentration between H-atoms and a region of depletion between O-atoms. As  $d(\text{H--H})$  increases, the first order change reduces to one critical point, and only a region of concentration (spanning over all three interactions) is seen in the 2<sup>nd</sup> order change. Strikingly, the general pattern of topology remains relatively constant across all values of  $d(\text{H--H})$ ; only the relative values differ in the second order change at  $d(\text{H--H}) = 2.8$  Å (where only concentration is observed) and at  $d(\text{H--H}) = 1.6$  Å showing that the same mechanisms governing the electron distribution are present for the range of  $d(\text{H--H})$  examined in this study; the second order change is always lowest between H-atoms. This point is emphasized by examining the cross-sections of the deformation density for **d4**, as shown in Figure 6 (and for **d3** in Figure S10 in the SI). At short  $d(\text{H--H})$ , a clear inflow and outflow of density is observed for the H•••H and O•••O interaction, respectively. As  $d(\text{H--H})$  increases, the interplay between an outflow of density from the interatomic region of the H•••H interactions and inflow of density into the bonding region of the O•••O interaction, gradually brings the accumulation peaks closer together which finally results in a net overall accumulation at  $d(\text{H--H}) = 2.8$  Å. It seems that the deformation density patterns (as well as the resulting patterns observed in the second order change of the molecular electron density) are primarily a result of the

kind of atoms involved, with the distance between them only determining the density at critical points and the net observed effect.

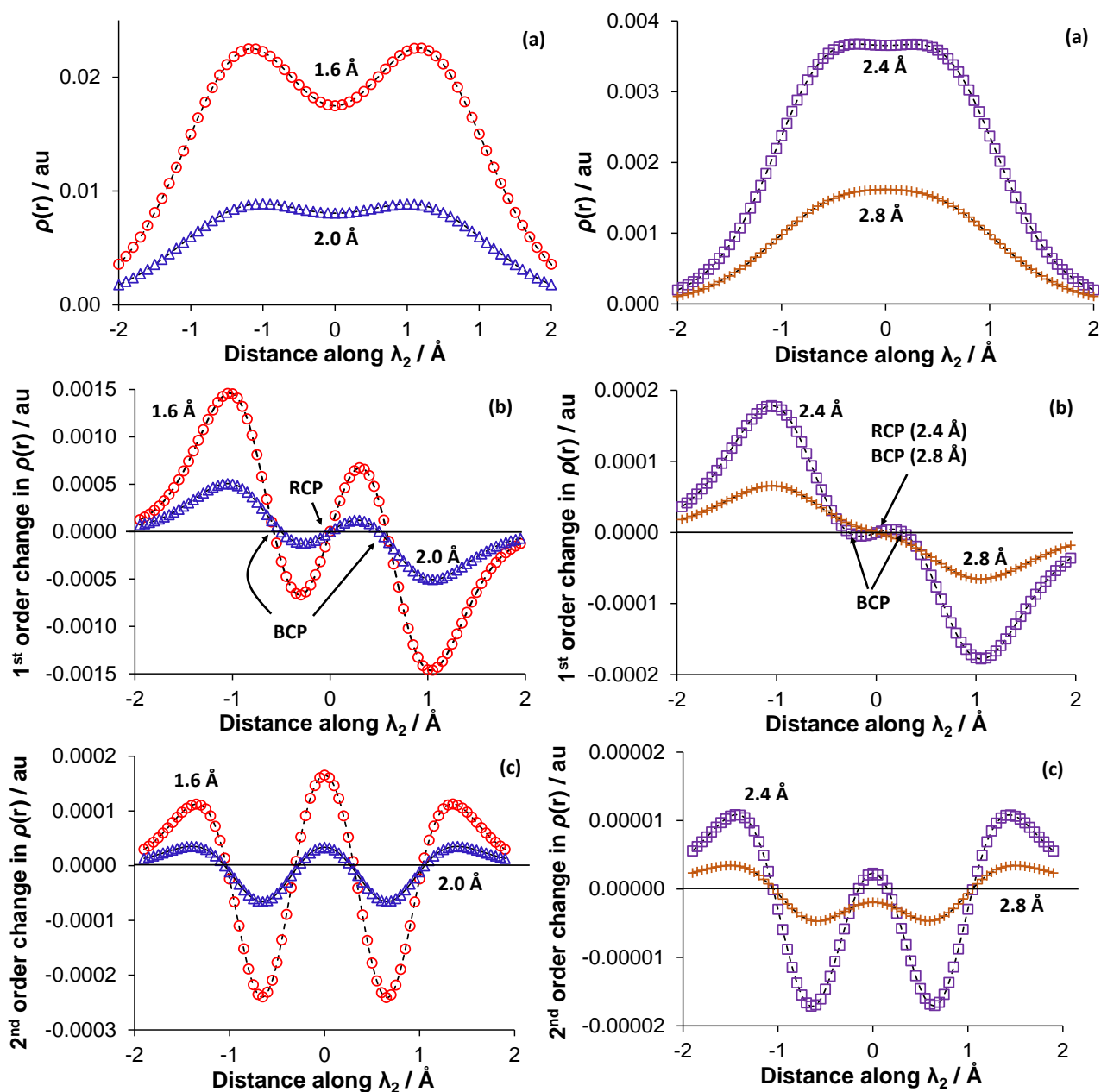


**Figure 5.** Cross-section of the a) electron density, b) its first and c) second order changes, along the  $\lambda_2$  eigenvector for  $d4$  for indicated distances of  $d(\text{H-H})$ . The origin of the cross-section is either RCP or BCP between O1 and O3 atoms.

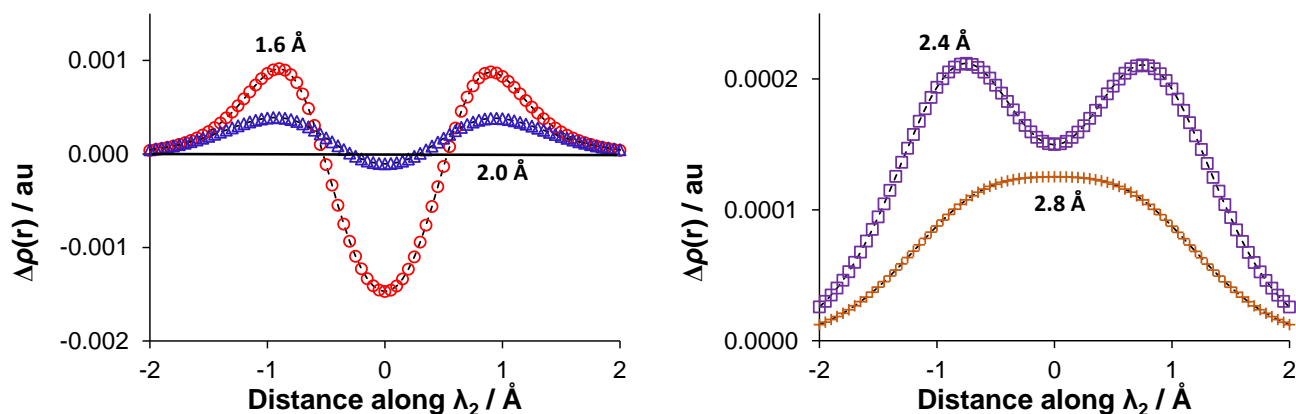


**Figure 6.** Cross-section of the deformation density along the  $\lambda_2$  eigenvector for indicated distances of **d4**. The origin of the vector is either RCP or BCP between O1 and O3 atoms.

From the above considerations and data shown in Table 1 it is clear that the presence of an AIL does not necessarily mean that:

- Atoms are involved in an attractive (or stabilizing) interaction with  $E_{\text{int}}^{\text{A,B}} < 0$ ; only in the case of O1 and H5 **d1** we observe an AIL and  $E_{\text{int}}^{\text{A,B}} < 0$ .
- The interaction is strongest among all, as measured by  $E_{\text{int}}^{\text{A,B}}$ , *e.g.*, in **d4** with  $d(\text{H5--H6}) = 1.6 \text{ \AA}$ , an AIL is observed between H-atoms involved in the weakest and repulsive interaction even though there is highly attractive and stronger interaction present in this molecular system (O1 $\cdots$ H5 with  $E_{\text{int}}^{\text{A,B}} = -103 \text{ kcal/mol}$ ).
- A positive density deformation (which shows an inflow of density into an interatomic region on the formation of an interaction) should be expected, *e.g.*, (i) in the case of **d2**, an outflow of density,  $\Delta\rho(\mathbf{r}) < 0$ , is observed between O-atoms linked by an AIL at any  $d(\text{O1},\text{O4})$ , or (ii) in the case of **d3** at  $d(\text{O1},\text{O4}) = 2.0 \text{ \AA}$ , one observes AIL between O1 and O4 while  $\Delta\rho(\mathbf{r}) < 0$ . Note that these two interactions exhibit highly repulsive character.

The analysis of deformation density,  $\Delta\rho(\mathbf{r})$ , provides not only an important insight on the mechanism of density distribution in the final structure of a molecular system but also might be more intuitive for a classical chemist in interpreting interactions in terms of bond formation. However:

- The sign of  $\Delta\rho(\mathbf{r})$  cannot be used to predict the character of an interaction in the final structure as there is no correlation between the signs of  $\Delta\rho(\mathbf{r})$ ,  $E_{\text{int}}^{\text{A,B}}$  and  $\lambda_2$ . For instance, an inflow of density,  $\Delta\rho(\mathbf{r}) > 0$ , and accumulated density in the interatomic region,  $\lambda_2 < 0$  (both indices are synonymous with a formation of a chemical bond or bonding interaction) is observed in (i) **d4**

for highly repulsive interactions  $H5\cdots H6$  at any distance and  $O1\cdots O3$  at  $d \geq 2.8 \text{ \AA}$ , as well as

- (ii) **d1** for highly attractive  $O1\cdots H5$  interaction, a classical intermolecular H-bond.
- b) An outflow of density, as predicted by  $\Delta\rho(\mathbf{r}) < 0$ , is not synonymous with either the repulsive interaction or a local *resultant* depletion in the density as indicated by  $\lambda_2 > 0$ . For instance, for  $\Delta\rho(\mathbf{r}) < 0$  we still observe  $\lambda_2 < 0$  for two interactions in **d3**, namely for highly repulsive  $O1\cdots O4$  with an AIL and highly attractive ( $E_{\text{int}}^{\text{A,B}} = -121 \text{ kcal/mol}$ )  $O1\cdots H5$  without an AIL.

### 3.2 Bipyridine

We change our focus from inter- to intramolecular interactions in *s-cis* and *s-trans* forms of bpy (L) and its protonated forms, HL and  $H_2L$  (signs are omitted for simplicity), because they provide many contacts of different nature which will allow us to examine the electron density distributions in different molecular as well as immediate environments. From the data shown in Table S2 and

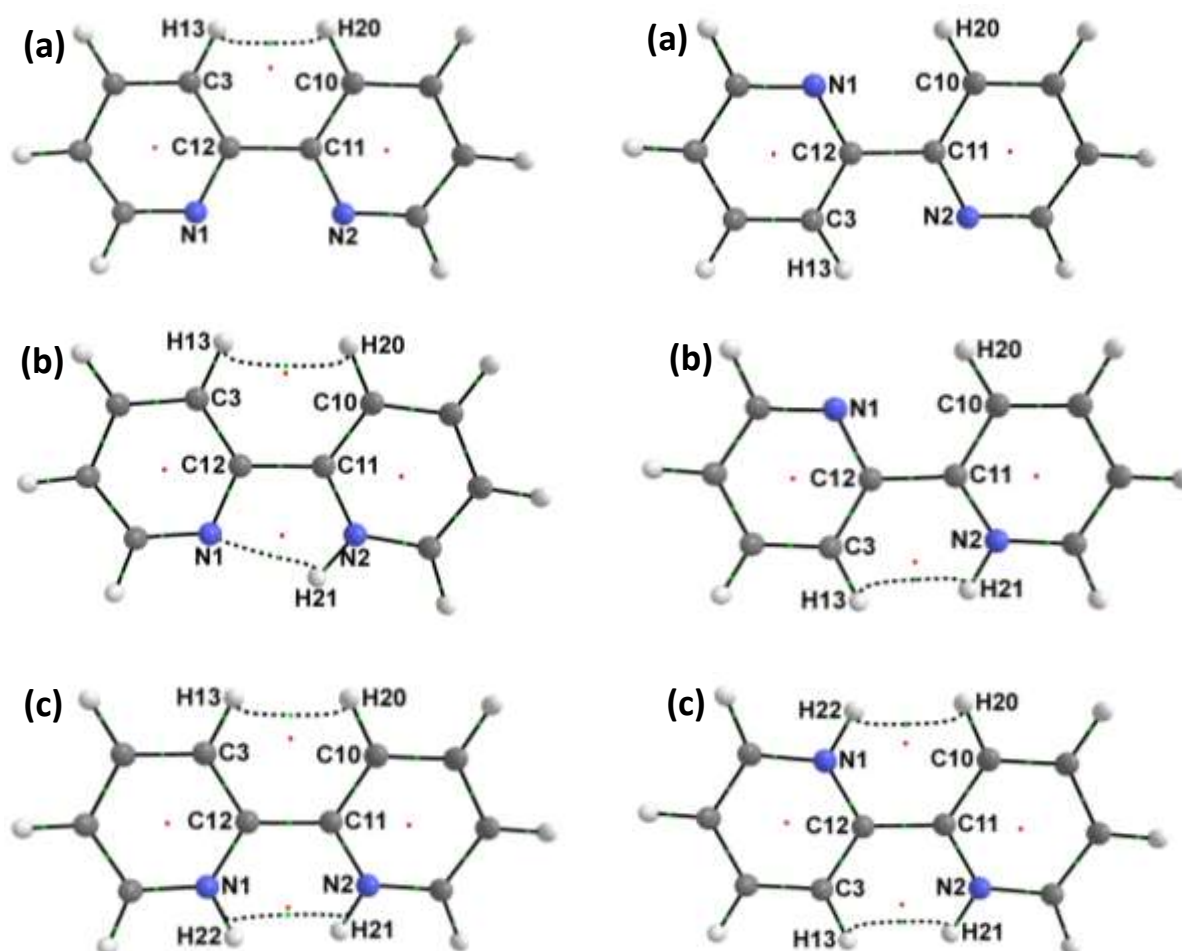


**Figure 7.** Molecular graphs of the *s-cis* and *s-trans* forms of a) bipyridine, L, b) HL and c)  $H_2L$ .



Figure S11 of the SI it follows that there are two genuine equilibrium structures among those examined here, namely *s-trans* L and *s-cis* HL. This means that we will be able to compare properties of intramolecular interactions formed by spontaneous change in the configuration of a molecule against forced-to-be contacts in non-equilibrium conformers obtained by rotating the rings along the N,C,C,N dihedral angle.

As shown in Figure 7, the molecular graphs do not exhibit AILs for all close contacts even though a distance criterion,  $d(A-B) < \text{sum of the van der Waals radii}$ , is met in all cases. From the NCI perspective (as shown in Figure 8 and Figures S12 of the SI), all contacts show regions where the reduced density gradient approaches zero, indicative of atoms being involved in an interaction.

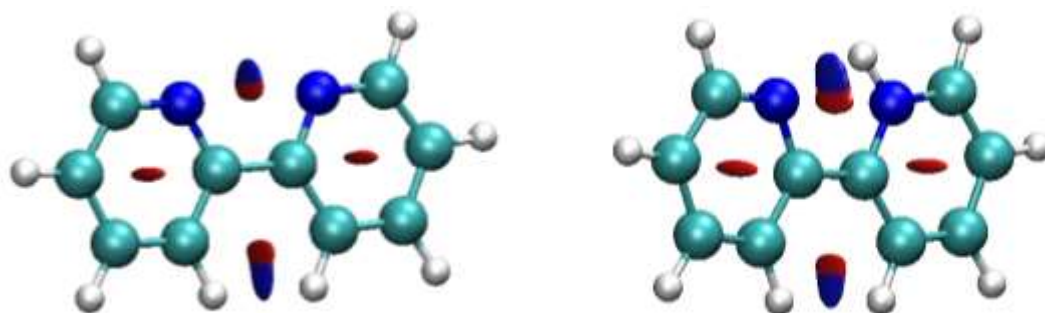


**Figure 8.** NCI isosurfaces of the *s-cis* forms of bpy (L) and HL, with a RDG isovalue = 0.5 au and isosurfaces coloured from blue to red using  $-0.03 \leq \rho(r) \times \text{sign}(\lambda_2) \leq +0.03$  au.

It was then of importance to examine the cross-sections of the electron density and results obtained for selected interactions without an AIL are shown in Figure 9a, and those with AIL are shown in Figure 9b (corresponding first- and second-order changes are shown in Figures S13 and S14 of the SI). Focusing on contacts without AILs, the CH...N interaction in *s-trans* L shows a clear concentration in the bonding region, but it is not sufficient to increase the density relative to a preceding point, hence no AIL is observed; this is a common feature for all interactions where density is locally increased but an AIL is not present. A very useful picture is obtained for the N...N interaction in *s-cis* L; it can be seen that exactly in the bonding region the density is only depletive and it increases somewhat outside the ring and this correlates well with the relevant NCI isosurface shown in Figure 8.

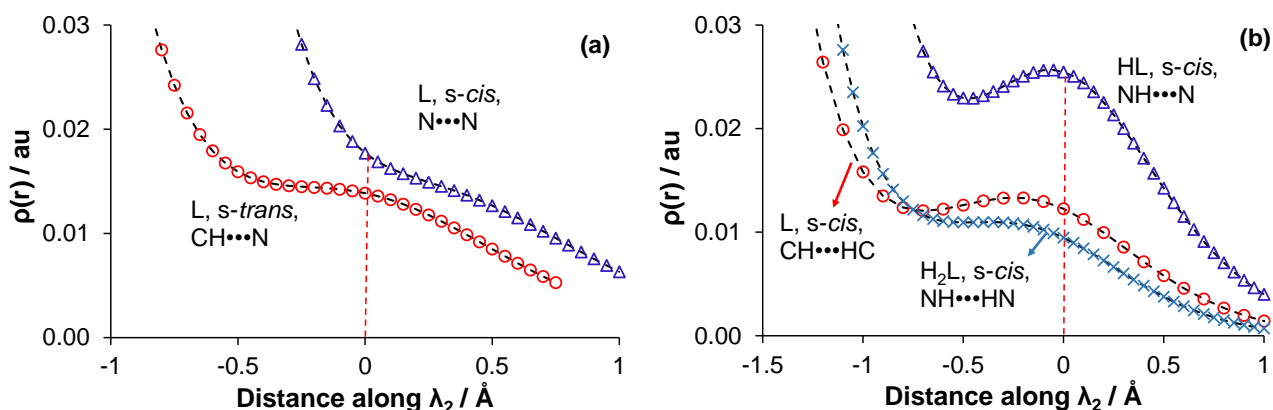


**Figure 9.** Cross-sections of the electron density along the  $\lambda_2$  eigenvector for indicated interactions (a) without a bond path, and (b) with a bond path present, in indicated forms of bpy. Dashed red line indicates Geometric Interaction Point (GIP) - point of lowest density directly between two atoms.

Regarding interactions with AILs, we always observe an increased density in the bonding region; this is clearly visible for the  $\text{NH}\cdots\text{N}$  (most pronounced change) and  $\text{CH}\cdots\text{HC}$  interactions in *s-cis* L, but only a very slight increase is seen for the  $\text{NH}\cdots\text{HN}$  interaction in *s-cis*  $\text{H}_2\text{L}$ . One can also observe that the maximum density (which correlates with a BCP) is shifted inside the respective ring from the GIP - point of lowest density directly between two nuclei.

The most informative picture is again observed for the cross-sections of the deformation density, although some care must be taken in the case of intramolecular interactions, since the fragments used to generate the deformation density (in this case, radical pyridine fragments) are unphysical reference states. However, even using fragments which are unlikely to exist in reality, the protocol used here is similar to that employed in frequently utilized energy decomposition techniques, such as ETS [65] and EDA [66]; hence, it should provide sufficient information to make qualitative conclusions related to the nature of these interactions.

Figure 10(a) shows the deformation densities for the  $\text{CH}\cdots\text{N}$  and  $\text{N}\cdots\text{N}$  interactions in *s-trans* and *s-cis* bpy, respectively, which are not linked by an AIL; an outflow of density from the bays as well as from the bonding interatomic regions is observed. The very repulsive  $\text{N}\cdots\text{N}$  interaction shows a maximum decrease in density within the  $\text{N}\cdots\text{N}$  bonding region, clearly showing that it is preferable to remove density from the electron-rich  $\text{N}\cdots\text{N}$  interaction upon its formation. This observation correlates well with the nature of this interaction as well as chemists' intuition, hence gives some credibility of this analysis, even though unphysical reference states were used. On the other hand, for the  $\text{CH}\cdots\text{N}$  interaction, the density depletion is greatest between the N1 and C10 atoms of the bay, and is approaching zero outside the bonding region.

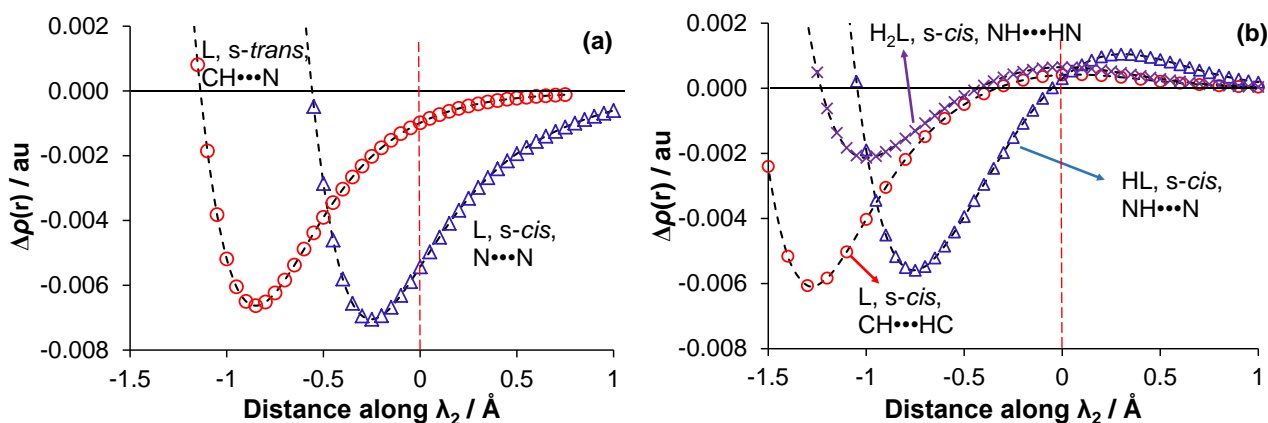


**Figure 10.** Cross-sections of the deformation density along the  $\lambda_2$  eigenvector for selected interactions (a) without bond path in deprotonated bpy and (b) with a bond path in indicated forms of bpy. Dashed red lines indicate the geometric interaction point, GIP.

Considering the deformation density cross-sections in Figure 10b for the  $\text{CH}\cdots\text{HC}$ ,  $\text{NH}\cdots\text{HN}$  and  $\text{NH}\cdots\text{N}$  interactions, all with an AIL present, a slight inflow of density is observed in the bonding region. This shows that, upon their formation, it is favourable to increase the density within these regions and in general, correlates well with the picture obtained from the analysis of the electron density cross-sections and the presence of AILs. However, using pyridine radical reference states, it is impossible to state with certainty whether density truly increases between these atoms in their interaction regions, but it is reasonable to infer that no significant density changes occur upon the formation of these interactions. On the other hand, it is important to note that a much larger and significant outflow of density takes place in the interatomic regions of neighbouring C- and N-atoms of the bay, as shown in Figure 10(b); this observation suggests that these atoms play larger roles than what is typically expected in the overall density distribution of the bay. In addition, the outflow of density in these neighbouring regions will significantly change the curvature of the electron density for the intramolecular interactions of interest, thereby possibly facilitating the appearance of AILs and regions of concentration. This concept is illustrated for the  $\text{CH}\cdots\text{HC}$  interaction in *s-cis* bpy in Figure S15 of the SI.

Finally, it is informative to discuss collated results shown in Table 2. There is only one case, the  $\text{N}\cdots\text{N}$  interaction in *s-cis* bpy, for which a fully consistent description emerges; it is characterized by a large repulsive interaction energy of +255.9 kcal/mol, absence of an AIL, a region of depleted density directly in the bonding region between the N-atoms ( $\lambda_2 > 0$ ) and an inflow of density takes place on its formation,  $\Delta\rho(\mathbf{r}) < 0$ . When these indices are combined, this interaction might be seen as a classic case of intramolecular repulsive steric contact. However, if this set of indices is used as a reference then the very electron-poor  $\text{NH}\cdots\text{HN}$  contact in *s-cis*  $\text{H}_2\text{L}$  (also with  $E_{\text{int}}^{\text{A,B}} \gg 0$ ) does not

conform to this criterion because density in the interatomic region is accumulated ( $\lambda_2 < 0$ ), an inflow of density takes place on the formation of this contact ( $\Delta\rho(\mathbf{r}) > 0$ ) and an AIL is linking H-atoms. It is obvious that using general chemical wisdom and intuition, these two contacts must be seen as destabilizing a molecule.

**Table 2.** Analysis of interactions in bpy and its protonated forms in terms of interaction energies and electron density in the interatomic region.

Molecule	Form	Interaction	Distance Å	$E_{\text{int}}^{\text{A,B}}$ <sup>a</sup>	$V_{\text{cl}}^{\text{A,B}}$ <sup>a</sup>	$V_{\text{XC}}^{\text{A,B}}$ <sup>a</sup>	AIL	$\rho(r) \times \text{sign}(\lambda_2)$ <sup>b</sup>	$\Delta\rho(r)_{\text{GIP}}$ <sup>c</sup>
bpy	<i>s-cis</i>	CH•••HC	1.98	-2.9	0.0	-3.0	Yes	-0.0123	+0.0004
		N•••N	2.72	255.9	264.4	-8.5	No	+0.0177	-0.0054
	<i>s-trans</i>	CH•••N	2.47	-14.7	-10.4	-4.3	No	-0.0139	-0.0010
Hbpy	<i>s-cis</i>	CH•••HC	2.19	-1.5	0.4	-1.9	Yes	-0.0083	+0.0004
		N•••HN	2.08	-128.3	-123.0	-5.4	Yes	-0.0255	+0.0005
	<i>s-trans</i>	CH•••HN	1.96	-0.7	1.1	-1.7	Yes	-0.0111	+0.0009
		CH•••N	2.43	-25.4	-20.9	-4.4	No	-0.0149	-0.0008
H <sub>2</sub> bpy	<i>s-cis</i>	CH•••HC	1.98	-1.5	1.2	-2.6	Yes	-0.0116	+0.0007
		NH•••HN	1.95	41.4	42.2	-0.9	Yes	-0.0095	+0.0006
	<i>s-trans</i>	CH•••HN	1.94	3.7	5.4	-1.7	Yes	-0.0118	+0.0009

<sup>a</sup> Diatomic interaction energies and decomposed components, all in kcal/mol; <sup>b</sup> Values in au at GIP; <sup>c</sup>The deformation density in au at GIP.

Let us analyse the CH--HC contacts which are often also seen as steric hindrance and became a subject of heated scientific debate when their nature in, *e.g.*, biphenyl goes [16,17,27–29,33,34]. We note with interest that in all three *s-cis* (de)protonated forms of bpy these contacts are characterized by the presence of AILs, favourable and XC-dominated interaction energy ( $E_{\text{int}}^{\text{A,B}} < 0$ ), an increased density in the interatomic region ( $\lambda_2 < 0$ ) and an inflow of density on these contacts formation; remarkably, this is exactly the same set of indices as observed for a spontaneous formation of a classical intermolecular H-bond in the water dimer *dI*.

Considering the CH•••N interactions, we found that they are characterized by a different set of descriptors when compared with those discussed for the CH--HC or NH--HN contacts. Also, the set of descriptors has not changed for the CH•••N interaction when going from the equilibrium *s-cis* L to non-equilibrium *s-trans* HL. Even though the CH•••N interactions contribute significantly more, when measured by the  $E_{\text{int}}^{\text{A,B}}$  term, to the overall stability of a molecule than the CH•••HC ones:

- a) Atoms involved in the interaction are not linked by an AIL even though density is accumulated,  $\lambda_2 < 0$
- b) An outflow of density takes place on the contact formation,  $\Delta\rho(\mathbf{r}) < 0$ .

An analysis of data shown in Table 2 also shows an influence of a molecular environment on the nature and strength of an interaction. For instance, we observe weakening of the CH•••HC interactions when going from unprotonated ( $E_{\text{int}}^{\text{A,B}} = -2.9$  kcal/mol) to diprotonated bpy ( $E_{\text{int}}^{\text{A,B}} = -1.5$  kcal/mol) and this is almost entirely due to an increase in a classical term from virtually zero in L to +1.2 kcal/mol in H<sub>2</sub>L. More apparent change, also mainly caused by an increase in the value of  $V_{\text{cl}}^{\text{A,B}}$ , involves the CH•••HN interaction which changed its nature from attractive in HL ( $E_{\text{int}}^{\text{A,B}} = -0.7$  kcal/mol) to repulsive in H<sub>2</sub>L ( $E_{\text{int}}^{\text{A,B}} = +3.7$  kcal/mol) even though in both cases  $\Delta\rho(\mathbf{r}) > 0$  and  $\lambda_2 < 0$  are observed between H-atoms involved with the  $V_{\text{XC}}^{\text{A,B}}$  term virtually unchanged.

In general, as observed for the water dimers, (i) there is no direct correlation between all indices discussed here, *e.g.*,  $E_{\text{int}}^{\text{A,B}} < 0$  or  $E_{\text{int}}^{\text{A,B}} > 0$  is not synonymous with the presence or absence of AIL, respectively, (ii) locally increased density, as identified by NCI, does not imply that this is the result of the density inflow into the interatomic region and also (iii) different mechanisms, through which electron density is distributed between atoms, also take place in case of intramolecular interaction.

### 3.3. NTPA

This common tetradentate ligand, has some conformational space in its free form but must undergo preorganization to form complexes with transition metals. It is known that on the complex formation the CH--HC steric contacts are present and this is commonly used to reason why NTPA forms weaker complexes with most metal ions than the slightly smaller (and less congested) NTA (nitritoltriacetic acid) [67–69]. We decided to examine here two, the lowest and highest energy, conformers of the free and deprotonated NTPA (LEC and HEC, respectively) and found several CH--HC contacts in both conformers but only one with an AIL - see Figure 11.

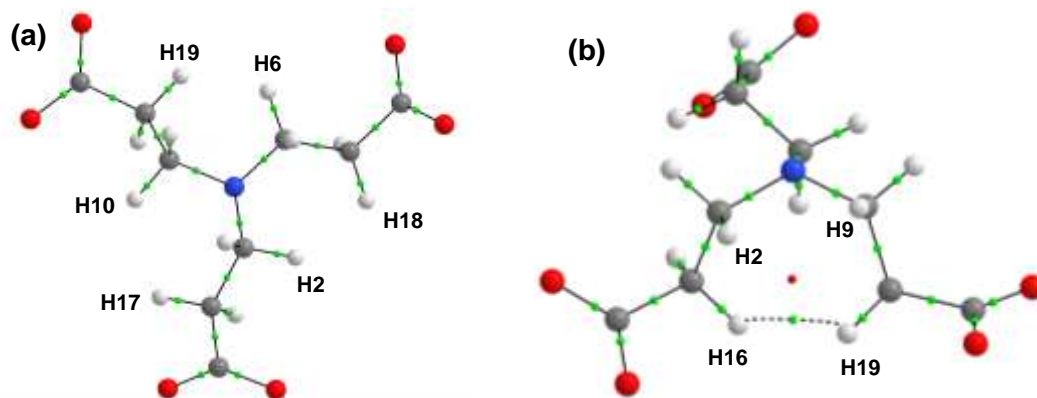


**Figure 11.** Molecular graphs of a) the lowest and b) highest energy conformer of NTPA.

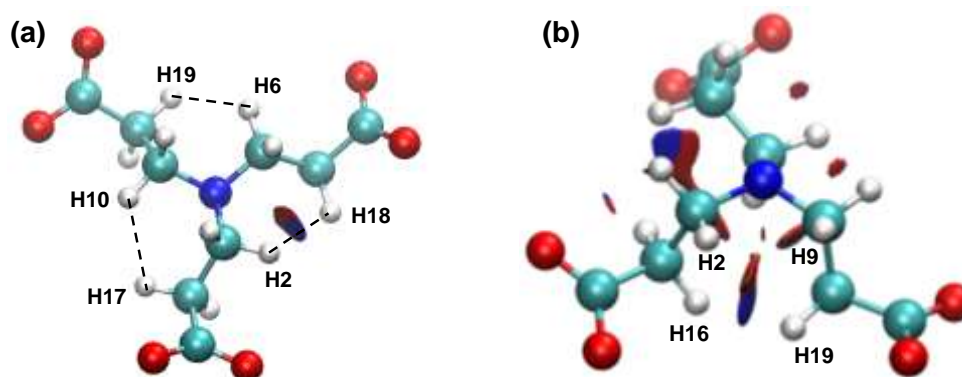


**Figure 12.** NCI analysis of NTPA conformers. (a) shows the lowest energy conformer and (b) shows the highest energy conformer. NCI regions are shown as blue and red surfaces, and isosurfaces coloured from blue to red using  $-0.03 \leq \rho(r) \times \text{sign}(\lambda_2) \leq +0.03$  au. The isosurface value is 0.5 au.

The number of the CH•••HC interactions presenting concentrated density within its bonding region was expanded upon NCI analysis (Figure 12) which also revealed two CH•••HC interactions in HEC which show only depletion. We therefore selected three examples of the CH•••HC interactions: (i) CH2•••H18C in LEC, which contains concentrated density but no AIL (note that there are three almost identical interactions of this type in LEC), (ii) CH16•••H19C in HEC, which contains concentrated density as well as an AIL, and (iii) CH2•••H9C in the HEC, which shows no AIL and only presents an NCI region of density depletion.

Interestingly, the IQA data (Table 3) reveals that all three interactions are attractive, with  $E_{\text{int}}^{\text{A,B}} = -3.3, -3.2$  and  $-1.6$  kcal/mol, respectively, and similarly to the CH•••HC interactions in all forms of bpy, they are dominated by the  $V_{\text{XC}}^{\text{A,B}}$  component.

**Table 3.** Analysis of interactions in the LEC and HEC of NTPA in terms of interaction energies and electron density in the interatomic region.

Form	Interaction	Distance Å	$E_{\text{int}}^{\text{A,B}}$ <sup>a</sup>	$V_{\text{cl}}^{\text{A,B}}$ <sup>a</sup>	$V_{\text{XC}}^{\text{A,B}}$ <sup>a</sup>	AIL	$\rho(r) \times \text{sign}(\lambda_2)$ <sup>b</sup>	$\Delta\rho(r)_{\text{GIP}}$ <sup>c</sup>
LEC	CH2•••H18C	2.11	-3.3	0.1	-3.4	No	-0.0105	-0.0007
HEC	CH16•••H19C	2.13	-3.2	0.1	-3.2	Yes	-0.0103	-0.0012
	CH2•••H9C	2.27	-1.6	0.2	-1.8	No	+0.0105	-0.0035

<sup>a</sup>Diatomic interaction energies and decomposed components, all in kcal/mol; <sup>b</sup>Values in au at GIP; <sup>c</sup>The deformation density in au at GIP.

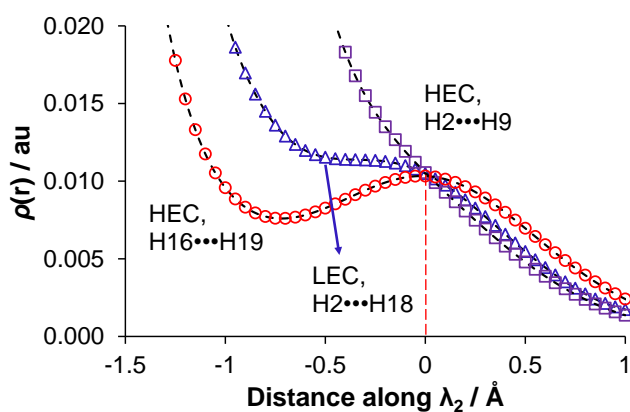


**Figure 13.** Cross-sections of the electron density along the  $\lambda_2$  eigenvector for indicated interactions in the lowest and highest energy conformers of NTPA. The dashed red line indicates the GIP.

Cross-sections of the electron density, as shown in Figure 13, revealed a few very interesting features. The electron density at GIP for each CH•••HC interaction is almost identical, with  $\rho(\mathbf{r}) \sim 0.01$  au. However, the topology of the interactions differ, predominantly in the region preceding the GIP. In CH16•••H19C, where an AIL is present, the neighbouring region shows the largest depletion, followed by CH2•••H18C, the interaction without an AIL but showing concentration in the bonding region. Finally, CH2•••H9C in HEC shows a mostly uniformly declining electron density, with no shoulder in the bonding region (and hence no concentration), but also no valley in the neighbouring regions (hence no AIL). It is thus clear that the appearance of concentration regions for these interactions is mostly dependant on the density distribution of the local environment.

Figure 14 shows the deformation density for the three CH•••HC interactions of NTPA. Surprisingly, all three interactions show somewhat negative deformation densities with the largest outflow from the bonding region of CH2•••H9C in HEC where identified by NCI depletion in density is observed but, like the CH•••HC interactions in bpy, the largest changes occur in

neighbouring regions. Regardless of the different mechanisms, however, in all cases these interactions exhibit  $E_{\text{int}}^{\text{A,B}} < 0$  and are almost entirely dominated by the  $V_{\text{XC}}^{\text{A,B}}$  term.

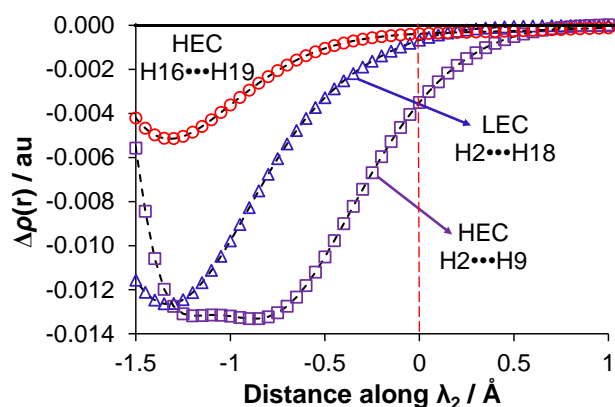


**Figure 14.** Cross-sections of the electron density distribution along the indicated interactions in the lowest and highest energy conformers of NTPA. Red dashed line indicates the GIP.

In general, there is no obvious correlation between the presence (or absence) of AIL and the signs of  $\Delta\rho(r)$ ,  $\lambda_2$  and  $E_{\text{int}}^{\text{A,B}}$  (as also observed for all other molecular systems discussed above), hence, the properties of topologies discussed here cannot be used to conclusively describe the chemical character of the CH--HC contacts or their impact on the stability of a molecule. Interestingly, however, these contacts exist already in the LEC of NTPA where, in principle, they could be avoided by just a slight rotation of the  $-\text{CH}_2-$  fragments but clearly that would result in some energy penalty: (i) either even larger strain than that caused by these contacts or (ii) the loss of three stabilizing CH•••HC interactions in LEC, amounting to  $-10$  kcal/mol.

#### 3.4. 2,2,2-tet

Triethylenetetramine (*trien*,) is a member of the homologous series of linear aliphatic polyamines (LAP), most of which are found in living organisms and play important roles in regulating cell proliferation and differentiation [70,71]. It is also a well-known copper chelator and has been used extensively in the treatment of Wilson's disease [72,73]. Due to the large conformational space available to this molecule, as well as the possibility of various intramolecular interactions (*e.g.*, NH•••N, CH•••HC, etc.) forming upon its protonation, we have found it suitable to study the electron density distributions of intramolecular interactions.

Figure 15 shows the molecular graphs of the lower (L1) and higher (L2) energy conformers. Both of them show a very strong (or leading) classical intramolecular NH•••N hydrogen bonds, with an AIL present, but these conformers differ in the overall congestion of the molecule. As a result, L1



forms an additional NH•••N interaction (with an AIL) and both conformers have additional CH•••HC and CH•••N interactions.

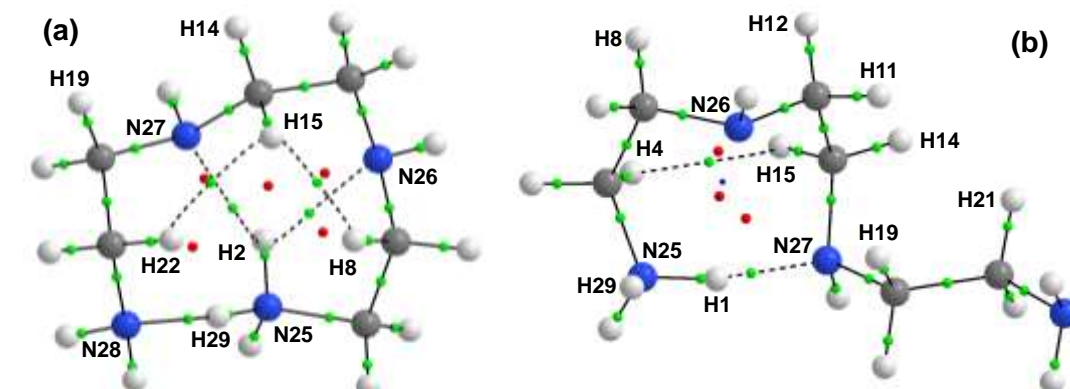


**Figure 15.** Molecular graphs of a) the lower energy L1 and b) higher energy L2 conformer of 2,2,2-tet.

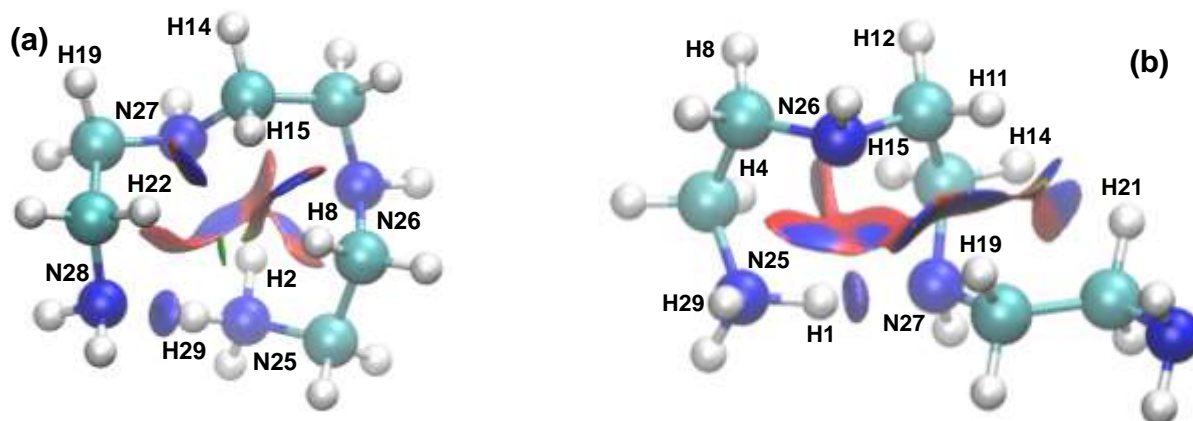


**Figure 16.** NCI isosurfaces of a) the lower L1 and b) higher energy L2 conformer of 2,2,2-tet with a RDG isovalue = 0.5 au and isosurfaces coloured from blue to red using  $-0.03 \leq \rho(r) \times \text{sign}(\lambda_2) \leq +0.03$  au.

The NCI-plots for each conformer, shown in Figure 16, disclose an abundance of intramolecular interactions involving N- and H-atoms. Focusing on the CH•••HC interactions, it can be seen that besides those with the presence of AILs, there also exist interactions just showing regions of concentration as well as regions of depletion.

Cross-sections of the electron density for the NH•••N, CH•••N and CH•••HC interactions are shown in Figures 17(a-c). A clear concentration and local maximum in the density is seen in L1 for the leading NH29•••N28 interaction, whilst only a slight increase in the density is observed for the weaker NH2•••N27 interaction; both maxima correspond to the observed BCP.

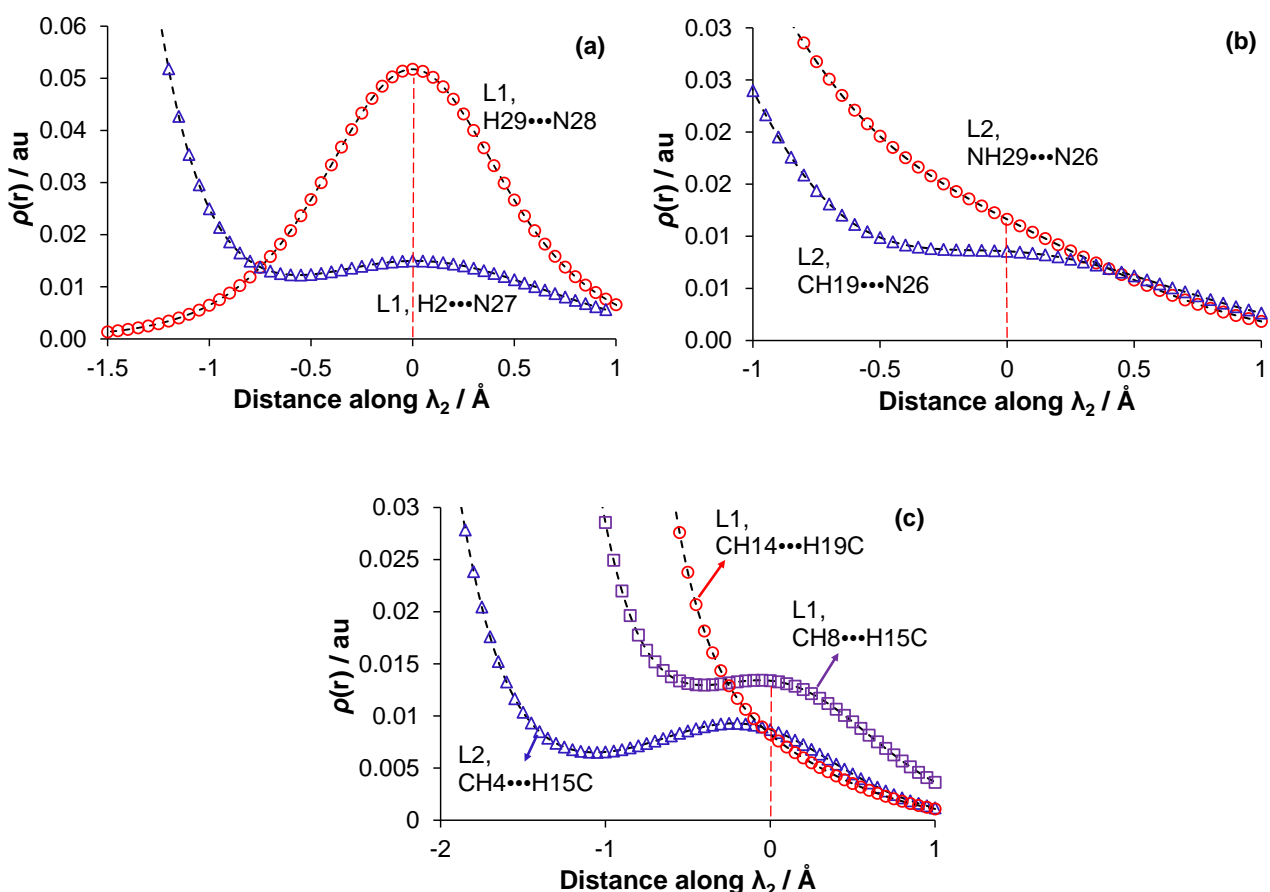


**Figure 17.** Cross-sections of the electron density along the  $\lambda_2$ -eigenvector for indicated a) H $\cdots$ N interactions with an AIL, b) XH $\cdots$ N interactions without an AIL and c) CH $\cdots$ HC interactions in the lower energy conformer, LEC, of 2,2,2-tet.

The difference between these two interactions, in terms of density cross-sections, might be rationalized in terms of the local environment; NH29 $\cdots$ N28 is on the ‘outskirts’ of a molecule, whereas NH2 $\cdots$ N27 occurs within the congested ring in the presence of numerous other interactions. For both interactions  $\Delta\rho(\mathbf{r}) > 0$ , but influence of the environment on the shape of the deformation densities can be easily deduced from Figure 18(a). Two other H $\cdots$ N interactions, CH19 $\cdots$ N26 and NH29 $\cdots$ N26 in L2, but without AILs present, are presented in Figure 17b. Regions of concentration and depletion are observed, respectively, but the deformation density cross-sections in Figure 18b show a very slight inflow of density for CH19 $\cdots$ N26 but only an outflow of density for NH29 $\cdots$ N26. A large spectrum of various H $\cdots$ N interactions with different indices are therefore observed in these molecules.

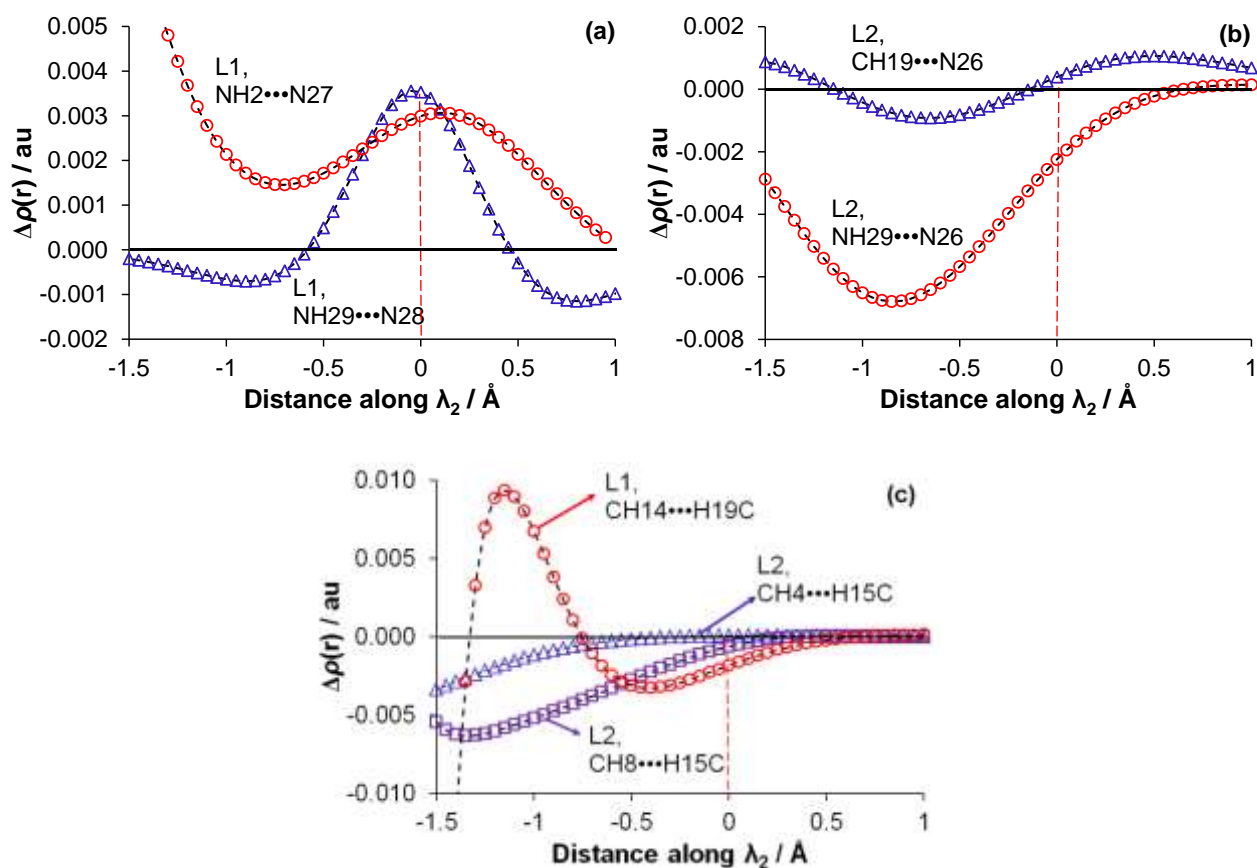


**Figure 18.** Cross-sections of the deformation density along the  $\lambda_2$ -eigenvector for indicated a) XH...N with AIL present, b) XH...N without AIL present and c) CH...HC interactions in the lowest energy conformer of 2,2,2-tet. Red dashed lines indicate the GIP.

The density cross-sections of selected CH...HC interactions (Figure 17c) show a variation similar to what was seen in NTPA, with clear increases in the electron density showing an AIL and the absence of any shoulders showing regions of depletion. The deformation densities (Figure 18c) show a slight outflow of density in the interaction regions but, like the CH...HC interactions in NTPA and bpy, much larger changes in the neighbouring regions between C atoms except for CH14...H19C, where the cross-section passes close to the lone pair of a nitrogen atom).

The full list of interacting atoms (as identified by NCI) is shown in Table 4, together with their IQA interaction energies. It is important to stress that, while the interaction energies of all intramolecular interactions vary greatly, there is not a single CH...HC interaction which is repulsive and all are showing dominating contribution of the  $V_{XC}^{A,B}$  term as found in bpy and NTPA; note that  $E_{int}^{A,B} < 0$  is observed in all molecular systems studied here, regardless whether density

concentration or depletion is observed in the bonding region, contradicting the MM-based notion of highly repulsive nature of this kind of interaction.

**Table 4.** Analysis of interactions in the protonated lower (L1) and higher (L2) energy conformers of 2,2,2-tet and its protonated forms in terms of interaction energies and electron density in the interatomic region.

Form	Interaction	Atoms A,B	Distance Å	$E_{\text{int}}^{\text{A,B}}$ <sup>a</sup>	$V_{\text{cl}}^{\text{A,B}}$ <sup>a</sup>	$V_{\text{XC}}^{\text{A,B}}$ <sup>a</sup>	AIL	$\rho(\mathbf{r}) \times \text{sign}(\lambda_2)$ <sup>b</sup>	$\Delta\rho(\mathbf{r})_{\text{GIP}}$ <sup>c</sup>
L1	NH...N	H29,N28	1.741	-131.8	-107.5	-24.3	Yes	-0.0517	+0.0035
	NH...N	H2,N27	2.379	-78.2	-73.5	-4.7	Yes	-0.0150	+0.0026
	NH...N	H2,N26	2.136	-89.8	-81.6	-8.2	Yes	-0.0239	+0.0000
	CH...HC	H8,H15	2.034	-3.6	+0.0	-3.6	Yes	-0.0134	-0.0006
	CH...HC	H15,H22	2.133	-3.0	+0.1	-3.1	Yes	-0.0098	+0.0000
	CH...HC	H14,H19	2.490	-0.9	+0.2	-1.1	No	+0.0082	-0.0018
L2	NH...N	H1,N27	1.654	-145.8	-116.5	-29.3	Yes	-0.0656	+0.0144
	NH...N	H29,N26	2.736	-61.4	-60.5	-0.9	No	+0.0116	-0.0022
	CH...N	H19,N26	2.711	-5.0	-1.9	-3.1	No	-0.0086	+0.0004
	CH...HC	H4,H15	2.156	-2.7	+0.1	-2.8	Yes	-0.0087	+0.0001
	CH...HC	H8,H12	2.426	-1.1	+0.2	-1.3	No	+0.0082	-0.0017
	CH...HC	H14,H21	2.273	-2.0	+0.1	-2.1	No	-0.0083	-0.0001
	CH...HC	H11,H19	2.344	-1.4	+0.1	-1.5	No	-0.0083	-0.0004
CH...HC	H11,H21	2.553	-0.9	+0.0	-1.0	No	-0.0045	-0.0000	

<sup>a</sup> Diatomic interaction energies and decomposed components, all in kcal/mol; <sup>b</sup> Values in au at GIP; <sup>c</sup>The deformation density in au at GIP.

All NH...N interactions are characterized by large and negative interaction energies but H29...N26 ( $E_{\text{int}}^{\text{A,B}} = -61.4$  kcal/mol in L2) does not have an AIL (most likely due to interatomic distance of 2.74 Å) and has a unique and somewhat unexpected set of NCI and deformation density indices, namely a local depletion in electron density ( $\rho(\mathbf{r}) \times \text{sign}(\lambda_2) = +0.0116$  au) and an outflow of density on this interaction formation is observed,  $\Delta\rho(\mathbf{r}) < 0$ . Furthermore, there is no significant inflow of density on the formation of the H2...N26 interaction in L1 even though it is the second strongest (in stabilizing manner), has large locally increased density ( $\rho(\mathbf{r}) \times \text{sign}(\lambda_2) = -0.0239$  au) and atoms involved are linked by the AIL. The data obtained for the NH...N interactions show that (i) positive values of ( $\rho(\mathbf{r}) \times \text{sign}(\lambda_2)$ ) and (ii) outflow or no change in the deformation density,  $\Delta\rho(\mathbf{r}) \leq 0$  are not synonymous with destabilizing interaction; hence, former describes the resultant local density distribution and the latter explains the process of the resultant density formation, in- or outflow of density on an interaction formation and both these indices illustrate how a molecular system has minimized its energy in terms of density distribution.

Similar observations, related to significance of  $\rho(\mathbf{r}) \times \text{sign}(\lambda_2)$  and  $\Delta\rho(\mathbf{r})$ , apply to CH...HC interactions, all characterized by  $E_{\text{int}}^{\text{A,B}} < 0$  with dominant  $V_{\text{XC}}^{\text{A,B}}$  term and various combinations of resultant local density and its formation. For instance, let us focus on two, H8...H15 and

H14•••H19 in L1, where an inflow of density is observed but only former has  $\rho(\mathbf{r}) \times \text{sign}(\lambda_2) < 0$  and AIL. In some other cases,  $\Delta\rho(\mathbf{r}) \sim 0$  but density is locally increased with either AIL present or not. From the analysis of weaker intramolecular interactions, as identified by NCI, it would also appear that density is preferentially removed from peripheral or long-distance contacts (H14--H19, H29--N26, H8--H12) in favour of contacts with shorter distances which are localised within a ring formed by the leading NH•••N interaction.

From a chemist perspective it would be of importance to understand parameters controlling relative stability of conformers. A first attempt might be made by comparing the strength of the leading and 'truly' chemical in nature intramolecular H-bond. Unfortunately, inspection of data in Table 4 reveals that this is not the case as all indices are in favour of the NH•••N interaction in the higher energy conformer for which we observe stronger by  $-14$  kcal/mol interaction, much more significant covalent contribution, by about  $-5$  kcal/mol, significantly larger density accumulation in the interatomic region (about  $-0.015$  au) which resulted from a large inflow of density. The only reasonable explanation we were able to come up with is the presence of three highly stabilizing NH•••N interactions in L1 whereas only two are observed in L2. However, if these were the only significant changes then L1 should be more stable, by  $\sim -100$  kcal/mol, than L2 but this is not the case. Hence, L1 must have paid some energy penalties (not reflected in Table 4) which largely reduced the decrease in the final energy of the L1 conformer. Clearly, any rigorous attempt to explain and quantify conformational preference is not an easy, if at all possible, task when polyatomic molecular structures are considered. In this regard, the NCI is very useful in identifying regions with increased density in the interatomic region from which additional and possibly significant interactions can be identified. However, the appearance of blue regions in the NCI plots must be always accompanied by red ones (with depleted density) and interpretation of significance of the latter might be more difficult for chemists' purposes, in terms of stabilizing or unfavourable character of an interaction, as exemplified by, e.g., the highly stabilizing H29•••N26 interaction in L2.

#### 4. Conclusions

Numerous inter- (in water dimers) and intramolecular (in (de)protonated forms of bpy, NTPA and singly protonated 2,2,2-tet) interactions of different kind (O•••H, NH•••N, CH•••HC, CH•••HN, NH•••HN, CH•••N, H•••H, O•••O and N•••N) were investigated by exploring topology of electron density in the interatomic regions using standard protocols as implemented in QTAIM, IQA and

NCI as well as density cross section along the eigenvector corresponding to the  $\lambda_2$  eigenvalue of the Hessian matrix, starting from the geometric interaction point (the lowest density directly between two nuclei). All these techniques are concerned with the properties of the resultant density distribution in a molecular system. To gain further insight, we have also implemented here an analysis of deformation density from which the process, inflow or outflow of density from fragments to the interatomic region of an interaction of interest in a molecule or molecular system could be uncovered. Our main interest was to find out whether there are well-defined relationships between (i) QTAIM-defined an atomic interaction line, AIL (presence or absence), (ii) IQA-defined interaction energy,  $E_{\text{int}}^{\text{A,B}}$ , and its components, classical  $V_{\text{cl}}^{\text{A,B}}$  and exchange-correlation term  $V_{\text{XC}}^{\text{A,B}}$ , (iii) NCI-defined isosurfaces used to identify local regions of accumulated ( $\lambda_2 < 0$ ) or depleted ( $\lambda_2 > 0$ ) density relative to immediate environment, and (iv) deformation density which for  $\Delta\rho(\mathbf{r}) > 0$  indicates an inflow and  $\Delta\rho(\mathbf{r}) < 0$  indicates an outflow of density on the interaction formation.

The analysis of data presented in Table 5, where a full set of combined indices obtained for all interactions is shown, leads us to the following final conclusions:

- the presence of an AIL is observed for many interactions, regardless whether (i) they are highly attractive or repulsive as measured by the value and sign of  $E_{\text{int}}^{\text{A,B}}$ , (ii) an inflow or outflow of density takes place into the interatomic region
- there is no correlation between the signs of  $\lambda_2$  and  $E_{\text{int}}^{\text{A,B}}$ ; both, highly repulsive and attractive, interactions might have locally depleted density and *vice versa*,
- locally accumulated density, with  $\lambda_2 < 0$ , does not imply that this is the result of an inflow ( $\Delta\rho(\mathbf{r}) > 0$ ) or outflow of density, and this equally applies to attractive and repulsive interactions either with or without an AIL

From a chemist's perspective:

- the first three interactions in Table 5 can be interpreted as H-bonds (either inter- or intramolecular) and they all are characterized by the presence of AIL,  $E_{\text{int}}^{\text{A,B}} \ll 0$  dominated by the  $V_{\text{cl}}^{\text{A,B}}$  term,  $\lambda_2 < 0$  and  $\Delta\rho(\mathbf{r}) > 0$ . There are also other two interactions, CH...HC and CH...HN which have exactly the set of indices (but their interaction energy is dominated by the  $V_{\text{XC}}^{\text{A,B}}$ ) and classically the former is interested as steric hindrance and the latter as another kind of a H-bond.
- the last two interactions in Table 5 represent classical non-bonded and repulsive contacts which are characterized by the absence of AIL,  $E_{\text{int}}^{\text{A,B}} \gg 0$  dominated by the  $V_{\text{cl}}^{\text{A,B}}$  term, locally depleted density ( $\lambda_2 < 0$ ) and an outflow of density from the interatomic region ( $\Delta\rho(\mathbf{r}) > 0$ ). One must note

that there are also attractive interactions ( $E_{\text{int}}^{\text{A,B}} < 0$ ) without AILs, for which also locally depleted density and outflow of density from the interatomic region is observed, and one of them, NH•••N in 2,2,2-tet, would easily be interpreted as an intramolecular H-bond.

- the O•••O interaction in d4 is highly repulsive and would be classified by any chemist as highly destabilizing a molecular system but, at the same time, is characterized by three identical topological features as found for classical H-bonds, namely (i) the presence of an AIL, locally increased density in and an inflow into the interatomic region.
- the molecular environment can change the description, hence a character, of an interaction radically as exemplified by CH•••HC for which the set of descriptors varies from that observed in the case of classical H-bonds and changes to the set characterizing a destabilizing a molecule interaction, except the interaction energy between H-atoms involved which is always negative.
- none of the indices (IQA, QTAIM etc...), either separately or combined, can be used to predict the (de)stabilizing nature of an interaction except two limiting cases, the first and last interaction shown in Table 5.

The interpretation that the signs of  $\lambda_2$  or  $\Delta\rho(\mathbf{r})$  can be used as indications of “stabilizing”, “attractive” or even “bonding” rests on the concept that an increase in density in the bonding region of an interaction is an indication of a bonding mechanism. In this work, we have presented two different techniques to measure an increase in density in the bonding region: the sign of  $\lambda_2$  (as it is used in NCI and the interpretation of an AIL) and the sign of  $\Delta\rho(\mathbf{r})$ . The former indicates increased density relative to the local environment of an interaction, whereas the latter indicates increased density relative to non-interacting fragment states. We note that the combination of the two methods gives a much greater insight into the electron distribution of inter- and intramolecular interactions; this is particularly true for all of the CH•••HC interactions investigated in this work. Even though the electron density distributions of these interactions show a wide range of different indices, we note that, in cases where a concentration of density or even an AIL is seen, a large outflow of density is observed between the neighbouring C-atoms.

**Table 5.** Comparative analysis of all interactions investigated in this work.<sup>a</sup>

Structure	Interaction	Dominant term	$\lambda_2$	$\Delta\rho(r)_{\text{GIP}}$
Attractive ( $E_{\text{int}}^{\text{A,B}} < 0$ ) with AIL				
<i>d1</i>	O•••H	$V_{\text{cl}}$	neg	pos
L1 2,2,2-tet	NH•••N	$V_{\text{cl}}$	neg	pos
<i>s-cis</i> Hbpy	NH•••N	$V_{\text{cl}}$	neg	pos
<i>s-cis</i> bpy				
<i>s-cis</i> Hbpy				
<i>s-cis</i> H <sub>2</sub> bpy	CH•••HC	$V_{\text{XC}}$	neg	pos
L1 2,2,2-tet				
L2 2,2,2-tet				
<i>s-trans</i> Hbpy	CH•••HN	$V_{\text{XC}}$	neg	pos
HEC NTPA				
L1 2,2,2-tet	CH•••HC	$V_{\text{XC}}$	neg	neg
L2 2,2,2-tet				
Repulsive ( $E_{\text{int}}^{\text{A,B}} > 0$ ) with AIL				
<i>d4</i>	H•••H	$V_{\text{cl}}$	neg	pos
<i>d4</i>	O•••O	$V_{\text{cl}}$	neg	pos
<i>s-trans</i> H <sub>2</sub> bpy	NH•••HN	$V_{\text{cl}}$	neg	pos
<i>s-trans</i> H <sub>2</sub> bpy	CH•••HN	$V_{\text{cl}}$	neg	pos
<i>d2, d3</i>	O•••O	$V_{\text{cl}}$	neg	neg
<i>d4</i>	O•••O	$V_{\text{cl}}$	pos <sup>b</sup>	pos
Attractive ( $E_{\text{int}}^{\text{A,B}} < 0$ ) without AIL				
<i>d4</i>	O•••H	$V_{\text{cl}}$	neg	pos
L2 2,2,2-tet	CH•••N	$V_{\text{XC}}$	neg	pos
<i>s-trans</i> bpy				
<i>s-trans</i> Hbpy	CH•••N	$V_{\text{cl}}$	neg	neg
<i>d3 d4</i>	O•••H	$V_{\text{cl}}$	neg	neg
LEC NTPA				
L2 2,2,2-tet	CH•••HC	$V_{\text{XC}}$	neg	neg
L1 2,2,2-tet				
L2 2,2,2-tet	CH•••HC	$V_{\text{XC}}$	neg	~0
L2 2,2,2-tet	CH•••HC	$V_{\text{XC}}$	pos	neg
HEC NTPA				
L1 2,2,2-tet	CH•••HC	$V_{\text{XC}}$	pos	neg
L2 2,2,2-tet				
L2 2,2,2-tet	NH•••N	$V_{\text{cl}}$	pos	neg
Repulsive ( $E_{\text{int}}^{\text{A,B}} > 0$ ) without AIL				
<i>d4</i>	H•••H	$V_{\text{cl}}$	neg	pos
<i>d4</i>	O•••O	$V_{\text{cl}}$	pos	neg
<i>s-cis</i> bpy	N•••N	$V_{\text{cl}}$	pos	neg

<sup>a</sup> neg and pos stand for the negative and positive, respectively, signs of the  $\lambda_2$  and  $\Delta\rho(r)_{\text{GIP}}$  values; <sup>b</sup> this is at the GIP = RCP in this dimer where bifurcated AIL is observed



It appears that formation of an AIL does not have to be an output of the inflow of density into the interatomic region, as traced by the deformation density, but might be also an ‘artefact’ of density depletion between neighbouring atoms.

Clearly, care must be taken when using any *local* theoretical index (i.e. the value of the electron density or deformation density at a single coordinate), because the description of any interaction is highly influenced by its local environment. This is particularly true for congested systems, with many intramolecular interactions present in the same space. It is obvious that to fully uncover the chemical character of an interaction it would be necessary and informative to include additional physical properties and expand on methodologies used.

On a final note, we can also ask whether the presence of an AIL corresponds in any way with the delocalization or exchange interaction energy between competing pairs of atoms. Such a correspondence was suggested by Pendás et al, [38] and investigated in more detail by Tognetti and Joubert. [58] From the data obtained in this work, it would appear that Pendás’ interpretation of an AIL holds true – the interactions for which  $V_{XC}^{A,B}$  is the largest in magnitude does indeed show the presence of an AIL. For example, in **d1**,  $V_{XC}^{O1,H5} = -9.8$  kcal/mol, whereas  $V_{XC}^{O1,O4} = -4.9$  kcal/mol. However, we have found one case in **d4** with  $d(H-H) = 1.6$  Å, where the H••H interaction presenting an AIL has a less-negative  $V_{XC}^{A,B}$  value than its competing O••O interaction;  $V_{XC}^{H5,H6} = -2.6$  kcal/mol, whereas  $V_{XC}^{O1,O3} = -8.6$  kcal/mol. Whether this observation is a result of a structure which is far from equilibrium or whether it is a special case where Pendás’ interpretation (as determined by the methodology of Tognetti and Joubert) does not hold is a question we will investigate more thoroughly in the future.

## Acknowledgments

This work is based on the research supported in part by the National Research Foundation of South Africa (Grant Numbers 87777) and the University of Pretoria.

## 5. References

- [1] R.W.F. Bader, *Atoms in Molecules: A Quantum Theory*, Oxford University Press: Oxford, U.K., 1990.
- [2] E.R. Johnson, S. Keinan, P. Mori-Sánchez, J. Contreras-García, A.J. Cohen, W.J. Yang, Revealing Noncovalent Interactions, *Am. Chem. Soc.* 132 (2010) 6498–6506.

- [3] N. Gillet, R. Chaudret, J. Contreras-García, W. Yang, B. Silvi, J.P.J. Piquemal, Coupling quantum interpretative techniques: another look at chemical mechanisms in organic reactions, *Chem. Theory Comput.* 8 (2012) 3993–3997.
- [4] J. Contreras-García, E.R. Johnson, S. Keinan, R. Chaudret, J.P. Piquemal, D. Beratan, W.J. Yang, NCIPLOT: a program for plotting noncovalent interaction regions, *Chem. Theory Comput.* 7 (2011) 625–632.
- [5] P.L.A. Popelier, Quantum chemical topology: on bonds and potentials, in: D. Wales (Ed.), *Intermolecular Forces and Clusters I*, Springer-Verlag, Berlin, 2005, pp. 1–56.
- [6] N. Sukumar, C.M. Breneman, QTAIM in drug discovery and protein modelling, in: *The Quantum Theory of Atoms in Molecules: From Solid State to DNA and Drug Design*, C.F. Matta, R.J. Boyd (Eds.), Wiley-VCH Verlag GmbH & Co. KGaA, Weinheim, 2007, pp. 471–498.
- [7] M. Vafaezadeh, Z.B. Dizicheh, M.M. Hashemi, Mesoporous silica-functionalized dual Brønsted acidic ionic liquid as an efficient catalyst for thioacetalization of carbonyl compounds in water, *Catalysis Communications* 41 (2013) 96–100.
- [8] C.D.M. Churchill, D.M. Cassandra, L.R. Rutledge, S.D. Wetmore, Effects of the biological backbone on stacking interactions at DNA–protein interfaces: the interplay between the backbone  $\pi$  and  $\pi\pi$  components, *Phys. Chem. Chem. Phys.* 12 (2010) 14515–14526.
- [9] S.M. LaPointe, S. Farrag, H.J. Bohórquez, R.J. Boyd, QTAIM study of an  $\alpha$ -helix hydrogen bond network, *J. Phys. Chem. B* 113 (2009) 10957–10964
- [10] M. Mandado, A.M. Graña, R.A. Mosquera. Do 1, 2-ethanediol and 1, 2-dihydroxybenzene present intramolecular hydrogen bond?, *Phys. Chem. Chem. Phys.* 6 (2004) 4391–4396.
- [11] C.L. Firme, O.A.C. Antunes, P.M. Esteves, Relation between bond order and delocalization index of QTAIM, *Chem. Phys. Lett.* 468 (2009) 129–133.
- [12] U. Koch, P.L.A. Popelier, Characterization of CHO hydrogen bonds on the basis of the charge density, *J. Phys. Chem.* 99 (1995) 9747–9754
- [13] A.H. Pakiari, K. Eskandari, Closed shell oxygen–oxygen bonding interaction based on electron density analysis, *J. Mol. Struct: THEOCHEM* 806 (2007) 1–7.
- [14] R. F. W. Bader, Bond paths are not chemical bonds, *J. Phys. Chem. A* 113 (2009) 10391–10396.

- [15] L.J. Farrugia, C. Evans, M. Tegel, Chemical bonds without “chemical bonding”? A combined experimental and theoretical charge density study on an iron trimethylenemethane complex, *J. Phys. Chem. A* 110 (2006) 7952–7961.
- [16] J. Cioslowski, S.T. Mixon, Universality among topological properties of electron density associated with the hydrogen-hydrogen nonbonding interactions, *Can. J. Chem.* 70 (1992) 443–449.
- [17] J. Cioslowski, S.T. Mixon, Topological properties of electron density in search of steric interactions in molecules: electronic structure calculations on ortho-substituted biphenyls, *J. Am. Chem. Soc.* 114 (1992) 4382–4387.
- [18] H.A. Jimenez-Vazquez, J. Tamariz, R.J. Cross, Binding energy in and equilibrium constant of formation for the dodecahedrane compounds  $\text{He@C}_{20}\text{H}_{20}$  and  $\text{Ne@C}_{20}\text{H}_{20}$ , *J. Phys. Chem. A* 105 (2001) 1315–1319.
- [19] D. Moran, F. Stahl, E.D. Jemmis, H.F. Schaefer III, P.v.R. Schleyer, Structures, stabilities, and ionization potentials of dodecahedrane endohedral complexes, *J. Phys. Chem. A* 106 (2002) 5144–5154.
- [20] K. Kobayashi, S. Nagase, A stable unconventional structure of  $\text{Sc}_2\text{@C}_{66}$  found by density functional calculations, *Chem. Phys. Lett.* 362 (2002) 373–379.
- [21] A. Haaland, D.J. Shorokhov, N.V. Tverdova, Topological analysis of electron densities: is the presence of an atomic interaction line in an equilibrium geometry a sufficient condition for the existence of a chemical bond?, *Chem.–Eur. J.* 10 (2004) 4416–4421.
- [22] M.J. Jablonski, Energetic and geometrical evidence of nonbonding character of some intramolecular halogen⋯oxygen and other  $\text{Y}\cdots\text{Y}$  interactions, *Phys. Chem. A* 116 (2012) 3753–3764.
- [23] E. Cerpa, A. Krapp, R. Flores-Moreno, K.J. Donald, G. Merino, Influence of endohedral confinement on the electronic interaction between He atoms: A  $\text{He}_2\text{C}_{20}\text{H}_{20}$  case study, *Chem.–Eur. J.* 15 (2009) 1985–1990.
- [24] A.A. Popov, L. Dunsch, Bonding in endohedral metallofullerenes as studied by Quantum Theory of Atoms in Molecules, *Chem.–Eur. J.* 15 (2009) 9707–9729.
- [25] A.A. Popov, S.M. Avdoshenko, A.M. Pendás, L. Dunsch, Bonding between strongly repulsive metal atoms: an oxymoron made real in a confined space of endohedral metallofullerenes, *Chem. Commun.* 48 (2012) 8031–8050.

- [26] P. Dem'yanov, P. Polestshuk, A Bond Path and an Attractive Ehrenfest Force Do Not Necessarily Indicate Bonding Interactions: Case Study on  $M_2X_2$  ( $M = \text{Li, Na, K}$ ;  $X = \text{H, OH, F, Cl}$ ), *Chem.–Eur. J.* 18 (2012) 4982–4993.
- [27] J. Poater, M. Solà, F.M. Bickelhaupt, Hydrogen–Hydrogen bonding in planar biphenyl, predicted by Atoms-In-Molecules Theory, does not exist, *Chem.–Eur. J.* 12 (2006) 2889–2895.
- [28] J. Poater, M. Solà, F.M. Bickelhaupt, A model of the chemical bond must be rooted in quantum mechanics, provide insight, and possess predictive power, *Chem.–Eur. J.* 12 (2006) 2902–2905.
- [29] J. Poater, R. Visser, M. Solà, F.M. Bickelhaupt, Polycyclic benzenoids: why kinked is more stable than straight, *J. Org. Chem.* 72 (2007) 1134–1142.
- [30] A. Krapp, G. Frenking, Is This a Chemical Bond? A Theoretical Study of  $\text{Ng}_2@C_{60}$  ( $\text{Ng} = \text{He, Ne, Ar, Kr, Xe}$ ), *Chem. Eur. J.* 13 (2007) 8256–8270
- [31] S. Grimme, C. Mück-Lichtenfeld, G. Erker, G. Kehr, H. Wang, H. Beckers, H. Willner, When do interacting atoms form a chemical bond? Spectroscopic measurements and theoretical analyses of dideuteriophenanthrene, *Angew. Chem. Int. Ed.* 48 (2009) 2592–2595.
- [32] R.W.F. Bader, Autobiography of Richard FW Bader, *J. Phys. Chem. A* 115 (2011) 12432–12435.
- [33] C.F. Matta, J. Hernández-Trujillo, T.H. Tang, R.F.W. Bader, Hydrogen–Hydrogen bonding: a stabilizing interaction in molecules and crystals, *Chem.–Eur. J.* 9 (2003) 1940–1951.
- [34] R.F.W. Bader, Pauli repulsions exist only in the eye of the beholder, *Chem.–Eur. J.* 12 (2006) 2896–2901.
- [35] R.F.W. Bader, D.C. Fang, Properties of atoms in molecules: caged atoms and the Ehrenfest force, *J. Chem. Theory Comput.* 1 (2005) 403–414.
- [36] M. von Hopffgarten, G. Frenking, Chemical Bonding in the Inclusion Complex of He in Adamantane,  $\text{He}@ \text{adam}$ : Antithesis and Complement, *Chem.–Eur. J.* 14 (2008) 10227–10231.
- [37] A.M. Pendás, J. Hernández-Trujillo, The Ehrenfest force field: Topology and consequences for the definition of an atom in a molecule, *J. Chem. Phys.* 137 (2012) 134101–134102
- [38] A.M. Pendás, E. Francisco, M.A. Blanco, C. Gatti, Bond paths as privileged exchange channels, *Chem.–Eur. J.* 13 (2007) 9362–9371.

- [39] F. Weinhold, P. von Ragué Schleyer, W.C. McKee, Bay-type H $\cdots$ H “bonding” in cis-2-butene and related species: QTAIM versus NBO description, *J. of comp. chem.* 35 (2014) 1499–1508.
- [40] C. Foroutan-Nejad, S. Shahbazian, R. Marek, Toward a Consistent Interpretation of the QTAIM: Tortuous Link between Chemical Bonds, Interactions, and Bond/Line Paths, *Chem.–Eur J.* (2014) DOI:10.1002/chem.201402177.
- [41] S.J. Grabowski, J.M. Ugalde, Bond Paths Show Preferable Interactions: Ab Initio and QTAIM Studies on the X–H $\cdots$   $\pi$  Hydrogen Bond, *J. Phys. Chem. A.* 114 (2010) 7223–7229.
- [42] G. Frenking, M. Hermann, Critical comments on “One molecule, two atoms, three views, four bonds?”, *Angew. Chem.* 125 (2013) 6036–6039.
- [43] D. Danovich, S. Shaik, H.S. Rzepa, R. Hoffmann, A response to the critical comments on “One molecule, two atoms, three views, four bonds?”, *Angew. Chem. Int. Ed.* 52 (2013) 5926–5928.
- [44] I. Cukrowski, J.H. de Lange, M. Mitoraj, Physical Nature of Interactions in ZnII Complexes with 2, 2'-Bipyridyl: Quantum Theory of Atoms in Molecules (QTAIM), Interacting Quantum Atoms (IQA), Noncovalent Interactions (NCI), and Extended Transition State Coupled with Natural Orbitals for Chemical Valence (ETS-NOCV) Comparative Studies, *J. Phys. Chem. A* 118 (2014) 623–637
- [45] F. Weinhold, Natural bond critical point analysis: Quantitative relationships between natural bond orbital-based and QTAIM-based topological descriptors of chemical bonding, *J. Comp. Chem.* 33 (2012) 2440–2449.
- [46] J. Echeverría, G. Aullón, D. Danovich, S. Shaik, S. Alvarez, Dihydrogen contacts in alkanes are subtle but not faint, *Nat. Chem.* 3 (2011) 323–330.
- [47] R. Chaudret, B. de Courcy, J. Contreras-García, E. Gloaguen, A. Zehnacker-Rentien, M. Mons, J.P. Piquemal, Unraveling non-covalent interactions within flexible biomolecules: from electron density topology to gas phase spectroscopy, *Phys. Chem. Chem. Phys.* 16 (2014) 9876–9891.
- [48] A. Armstrong, R.A. Boto, P. Dingwall, J. Contreras-García M.J. Harvey, N.J. Masona, H.S. Rzepa, The Houk–List transition states for organocatalytic mechanisms revisited, *Chem. Sci.* 5 (2014) 2057–2071.
- [49] A. Otero-de-la-roza, R. Johnson, J. Contreras-garcía, Revealing non-covalent interactions in solids : NCI plots revisited, *Phys. Chem. Chem. Phys.* 14 (2012) 12165–12172.

- [50] R.F.W. Bader, A bond path: a universal indicator of bonded interactions, *J. Phys. Chem. A* 102 (1998) 7314–7323
- [51] J.C. Slater, Directed valence in polyatomic molecules, *Phys. Rev.* 37 (1931) 481–489.
- [52] J.C. Slater, *Quantum theory of molecules and solids*. Vol. 1. New York: McGraw-Hill, 1963, pp. 39–40.
- [53] R.P. Feynman, Forces in molecules, *Phys. Rev.* 56 (1939) 340–343.
- [54] W.L. Clinton, Forces in molecules. I. Application of the virial theorem, *J. Chem. Phys.* 33 (1960) 1603–1606.
- [55] J. Hernández-Trujillo, F. Cortés-Guzmán, D. Fang, R.F.W. Bader, Forces in molecules, *Faraday Disc.* 135 (2007) 79–95.
- [56] K. Ruedenberg, M.W. Schmidt, Why does electron sharing lead to covalent bonding? A variational analysis, *J. Comp. Chem.* 28 (2007) 391–410.
- [57] K. Ruedenberg, M.W. Schmidt, Physical Understanding through Variational Reasoning: Electron Sharing and Covalent Bonding, *J. Phys. Chem. A* 113 (2009) 1954–1968.
- [58] V. Tognetti, L. Joubert, On the physical role of exchange in the formation of an intramolecular bond path between two electronegative atoms, *J. Chem. Phys.* 138 (2013) 024102–024110.
- [59] M.A. Blanco, A.M. Pendás, E. Francisco, Interacting quantum atoms: a correlated energy decomposition scheme based on the quantum theory of atoms in molecules, *J. Chem. Theory Comput.* 1 (2005) 1096–1109.
- [60] E. Francisco, A.M. Pendás, M.A. Blanco, A molecular energy decomposition scheme for atoms in molecules, *J. Chem. Theory Comput.* 2 (2006) 90–102.
- [61] M. J. Frisch, G. W. Trucks, H. B. Schlegel, G. E. Scuseria, M. A. Robb, J. R. Cheeseman, G. Scalmani, V. Barone, B. Mennucci, G. A. Petersson, H. Nakatsuji, M. Caricato, X. Li, H. P. Hratchian, A. F. Izmaylov, J. Bloino, G. Zheng, J. L. Sonnenberg, M. Hada, M. Ehara, K. Toyota, R. Fukuda, J. Hasegawa, M. Ishida, T. Nakajima, Y. Honda, O. Kitao, H. Nakai, T. Vreven, J. A. Montgomery, Jr., J. E. Peralta, F. Ogliaro, M. Bearpark, J. J. Heyd, E. Brothers, K. N. Kudin, V. N. Staroverov, R. Kobayashi, J. Normand, K. Raghavachari, A. Rendell, J. C. Burant, S. S. Iyengar, J. Tomasi, M. Cossi, N. Rega, J. M. Millam, M. Klene, J. E. Knox, J. B. Cross, V. Bakken, C. Adamo, J. Jaramillo, R. Gomperts, R. E. Stratmann, O. Yazyev, A. J. Austin, R. Cammi, C. Pomelli, J. W. Ochterski, R. L. Martin, K. Morokuma, V. G. Zakrzewski, G. A. Voth, P. Salvador,

J. J. Dannenberg, S. Dapprich, A. D. Daniels, Ö. Farkas, J. B. Foresman, J. V. Ortiz, J. Cioslowski, and D. J. Fox, Gaussian 09, Revision D.1, Gaussian, Inc., Wallingford CT, 2009.

[62] T.A. Keith, AIMAll (Version 13.11.04), TK Gristmill Software, Overland Parks KS, USA, 2013 (aim.tkgristmill.com)

[63] W. Humphrey, A. Dalke, K. Schulten, VMD: visual molecular dynamics, *J. Molec. Graphics* 14.1 (1996) 33–38.

[64] Spartan'10, Wavefunction, Inc. Irvine, CA, 2010.

[65] M. Mitoraj, A. Michalak, T. Ziegler, A Combined Charge and Energy Decomposition Scheme for Bond Analysis, *J. Chem. Theory Comput.* 5 (2009) 962–975.

[66] K. Kitaura, K. Morokuma, A new energy decomposition scheme for molecular interactions within the Hartree-Fock approximation, *Int. J. Quantum Chem.* 10 (1976) 325-340.

[67] R.D. Hancock, A.S. De Sousa, G.B. Walton, J.H. Reibenspies, Metal-ion selectivity produced by C-alkyl substituents on the bridges of chelating ligands: The importance of short H-H nonbonded van der Waals contacts in controlling metal-ion selectivity. A thermodynamic, molecular mechanics and crystallographic study, *Inorg. Chem.* 46 (2007) 4749–4757.

[68] J.C.A. Boeyens, C.C. Fox, R.D. Hancock, Refinement of the structure of the nickel perchlorate complex of 1,4-diazacyclooctane,  $[\text{Ni}(\text{Daco})_2](\text{ClO}_4)_2 \cdot 2\text{H}_2\text{O}$  by empirical force-field methods, *Inorg. Chim. Acta* 87 (1984) 1–4.

[69] A.E. Martell, R.D. Hancock, *Metal Complexes in Aqueous Solutions*, Plenum Press, New York, 1996.

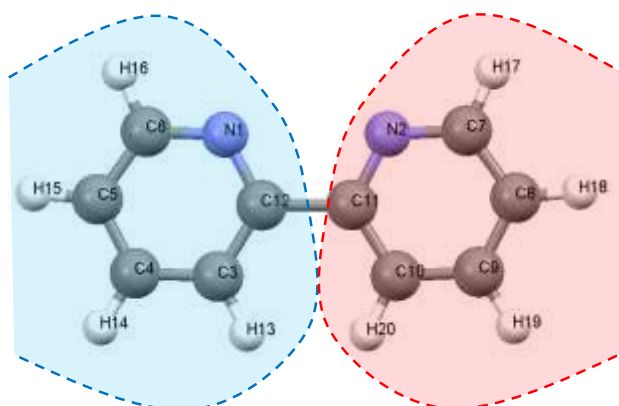
[70] E. Agostinelli, M.P.M. Marques, R. Calheiros, F.P.S.C. Gil, G. Tempera, N. Viceconte, V. Battaglia, S. Grancara, A. Toninello, Polyamines: fundamental characters in chemistry and biology, *Amino Acids* 38 (2010), 393–403.

[71] U. Bachrach, The early history of polyamine research, *Plant Phys. Biochem.* 48 (2010) 490–495

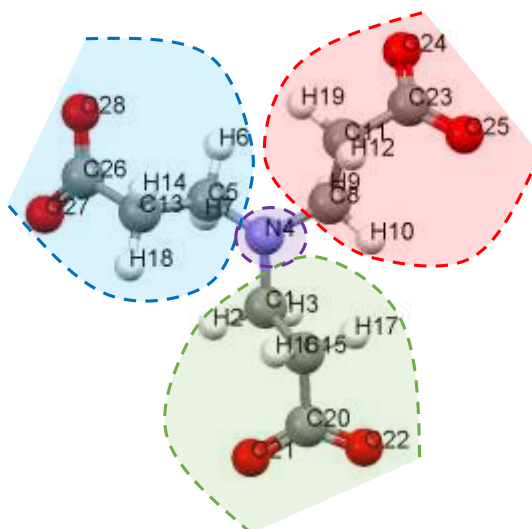
[72] L.A.E. Batisa de Carvalho, M.P.M. Marques, J. Tomkinson, Transverse Acoustic modes of biogenic and  $\alpha,\omega$ - polyamines: A study by inelastic neutron scattering and Raman spectroscopies coupled to DFT calculations, *J. Phys. Chem. A.* 110 (2006) 12947–12954.

[73] G.J.S. Cooper, Therapeutic Potential of Copper Chelation with Triethylenetetramine in Managing Diabetes Mellitus and Alzheimer's disease, *Drugs* 71 (2011) 1281–1320.

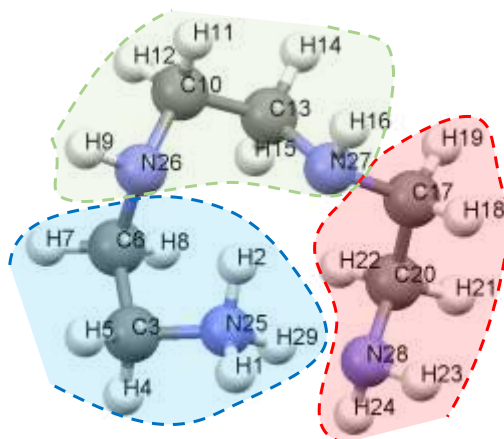
## Supplementary Information



**Figure S1.** Radical pyridine fragments used in the calculation of the deformation density in L, *s-cis* bipyridine.



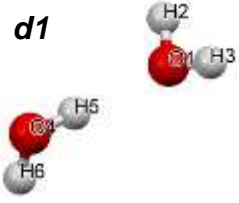
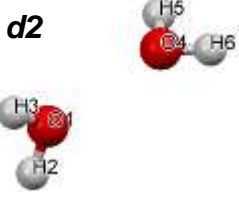
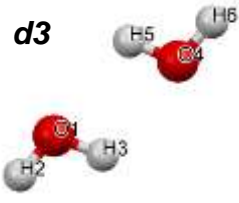
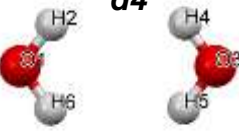
**Figure S2.** Radical fragments used in the calculation of the deformation density of the LEC of NTPA.

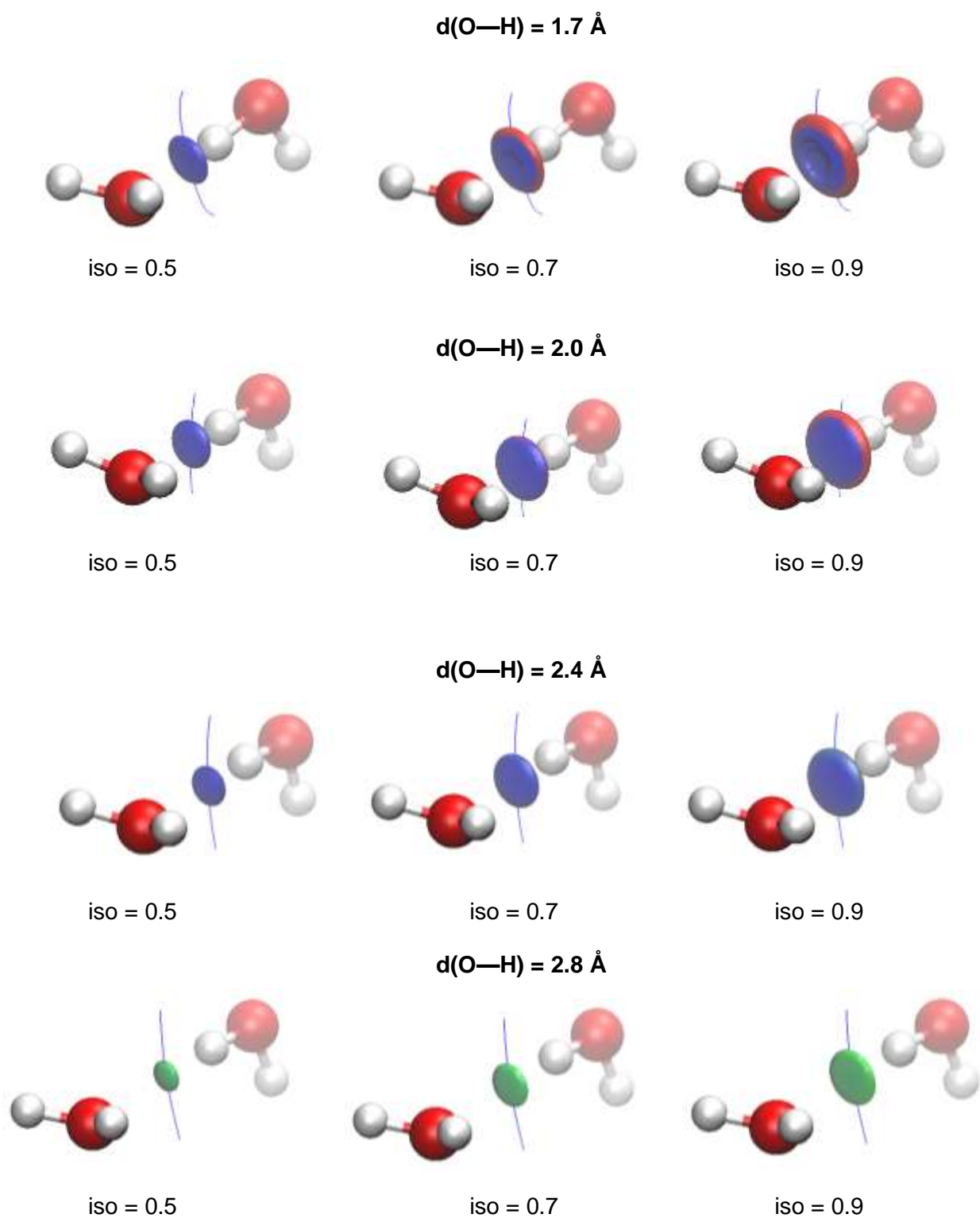


**Figure S3.** Radical fragments used in the calculation of the deformation density in the HEC of 2,2,2-tet.

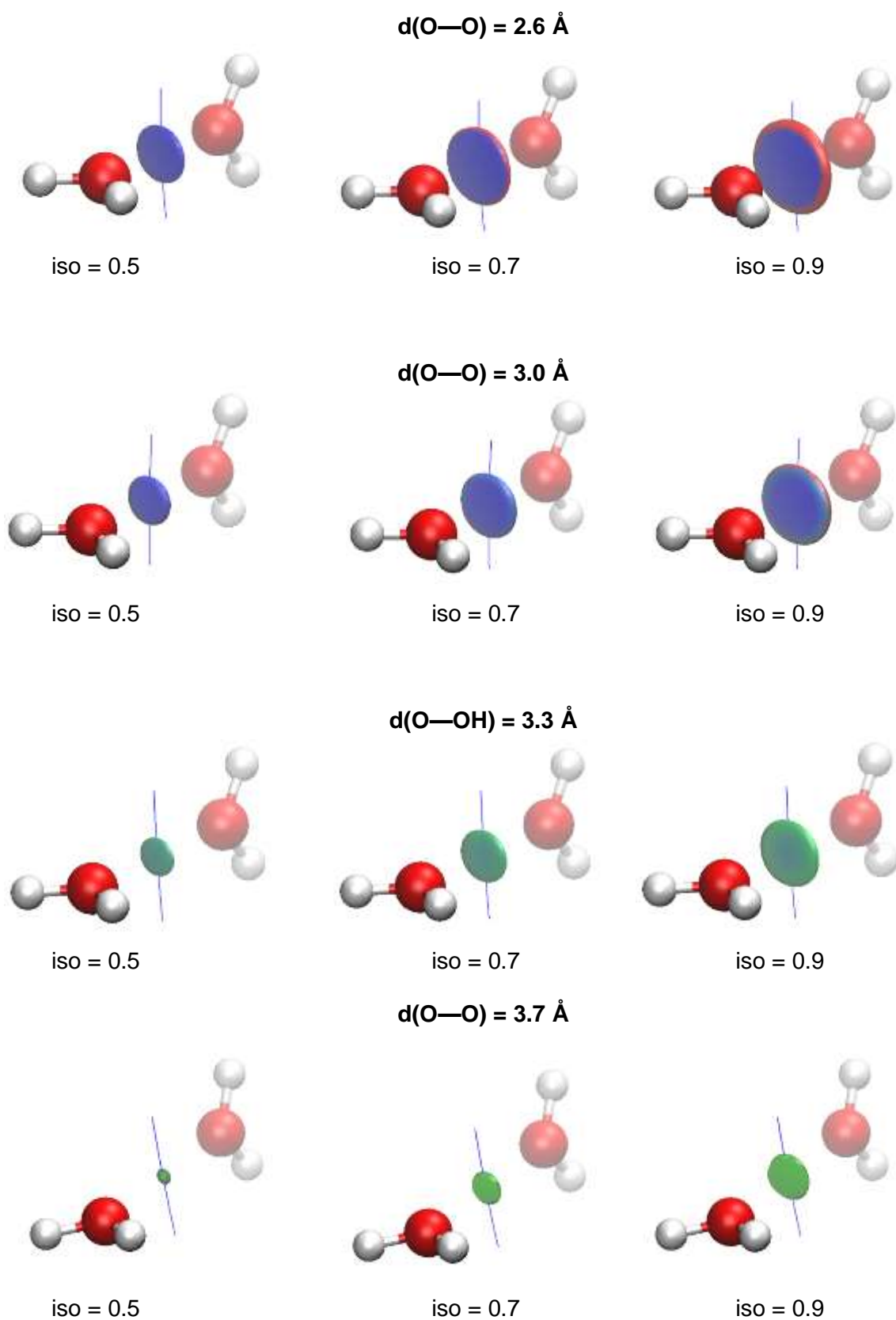


Table S1. Constrains applied during the optimization of water dimers

Dimer	Varied d(A--B)	Constraints applied during optimization
<p><b>d1</b></p> 	$1.8 \text{ \AA} \leq d(\text{H5--O1}) \leq 2.8 \text{ \AA}$	<p>d(H5--O1)</p> <p>At <math>d(\text{H5--O1}) = 2.8 \text{ \AA}</math>, <math>d(\text{O--O})</math> was kept fixed at <math>3.747 \text{ \AA}</math> in order to keep the same alignment of water molecules relative to each other.</p> <p><math>d(\text{O--O})</math></p>
<p><b>d2</b></p> 	$2.6 \text{ \AA} \leq d(\text{O1--O4}) \leq 4.0 \text{ \AA}$	<p><math>DA(\text{H3,O1,O4,H5}) = 90^\circ</math></p> <p><math>DA(\text{H3,O1,O4,H6}) = 90^\circ</math></p> <p><math>DA(\text{H2,O1,O4,H6}) = 90^\circ</math></p> <p><math>DA(\text{H2,O1,O4,H5}) = 90^\circ</math></p>
<p><b>d3</b></p> 	$2.0 \text{ \AA} \leq d(\text{O1--O4}) \leq 2.6 \text{ \AA}$	<p><math>d(\text{O--O})</math></p>
<p><b>d4</b></p> 	$1.6 \text{ \AA} \leq d(\text{H2--H4}) \leq 3.6 \text{ \AA}$	<p><math>d(\text{H--H})</math></p> <p>Only single point calculations could be performed on <b>d4</b>, with the water monomer used as reference for <math>d(\text{O--H})</math> bond lengths</p>



**Figure S4.** NCI-plots at various  $d(\text{O}-\text{H})$  for the *dI* water dimer, at indicated reduced density gradient isosurfaces. The isosurfaces are coloured from red to blue according to  $-1.0 \leq \lambda_2 \leq 1.0$  au.



**Figure S5.** NCI-plots at various  $d(\text{O}-\text{O})$  for the  $d2$  water dimer, at indicated reduced density gradient isosurfaces. The isosurfaces are coloured from red to blue according to  $-1.0 \leq \lambda_2 \leq 1.0$  au.

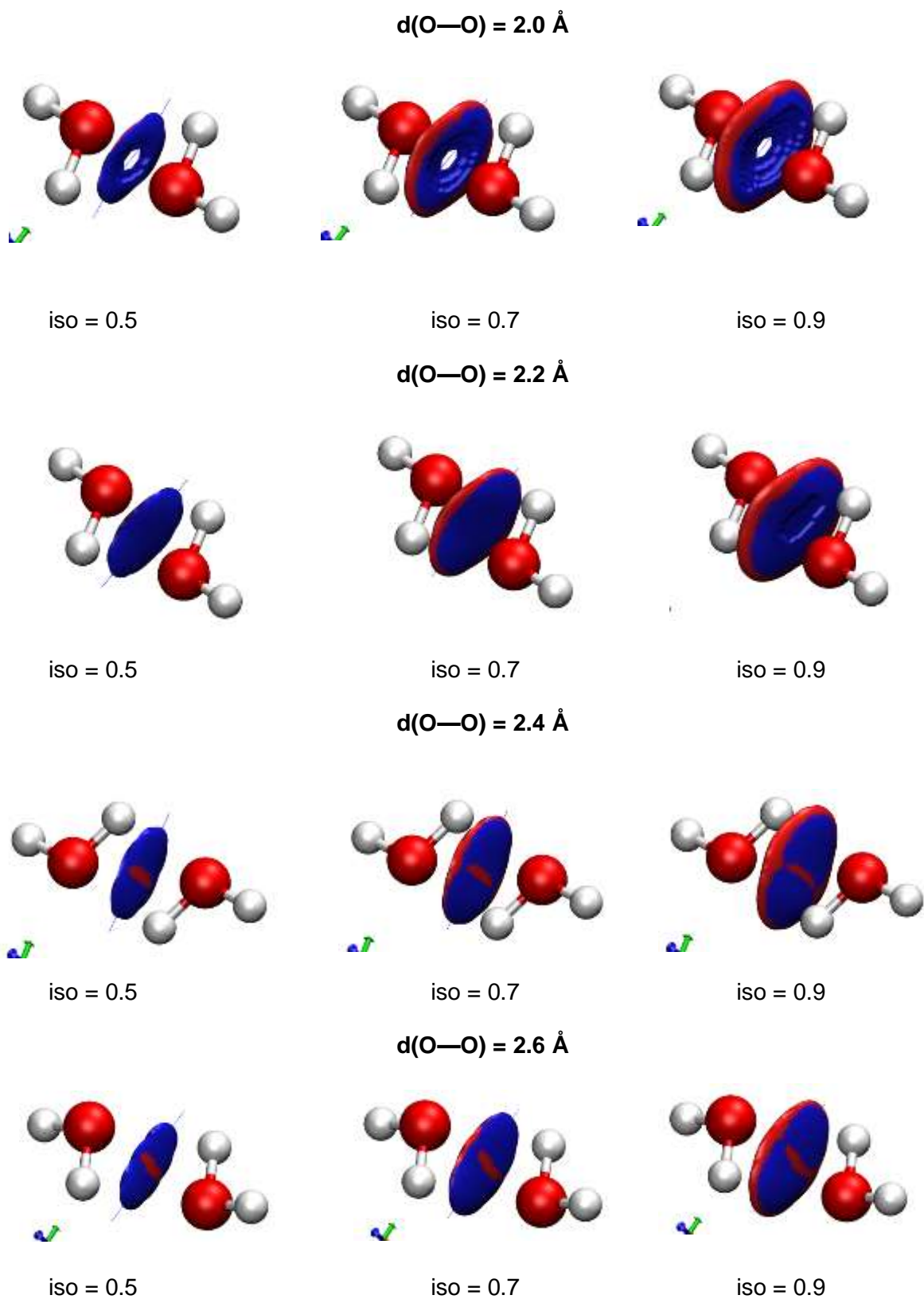


**Figure S6.** NCI-plots at various  $d(\text{O}-\text{O})$  for the  $d3$  water dimer, at indicated reduced density gradient isosurfaces. The isosurfaces are coloured from red to blue according to  $-1.0 \leq \lambda_2 \leq 1.0$  au.

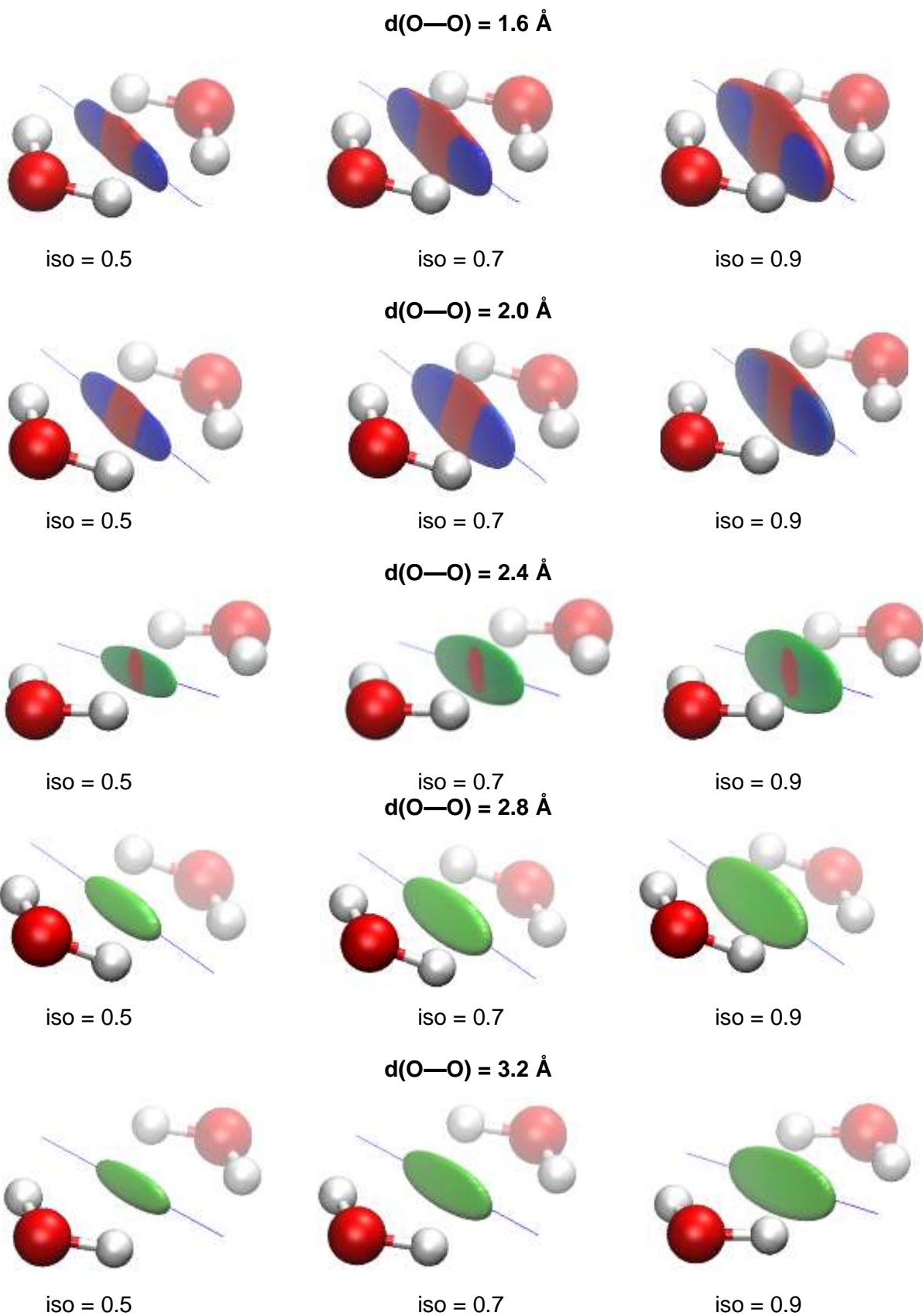


**Figure S7.** NCI-plots at various  $d(\text{H}-\text{H})$  for the  $d4$  water dimer, at indicated reduced density gradient isosurfaces. The isosurfaces are coloured from red to blue according to  $-1.0 \leq \lambda_2 \leq 1.0$  au.

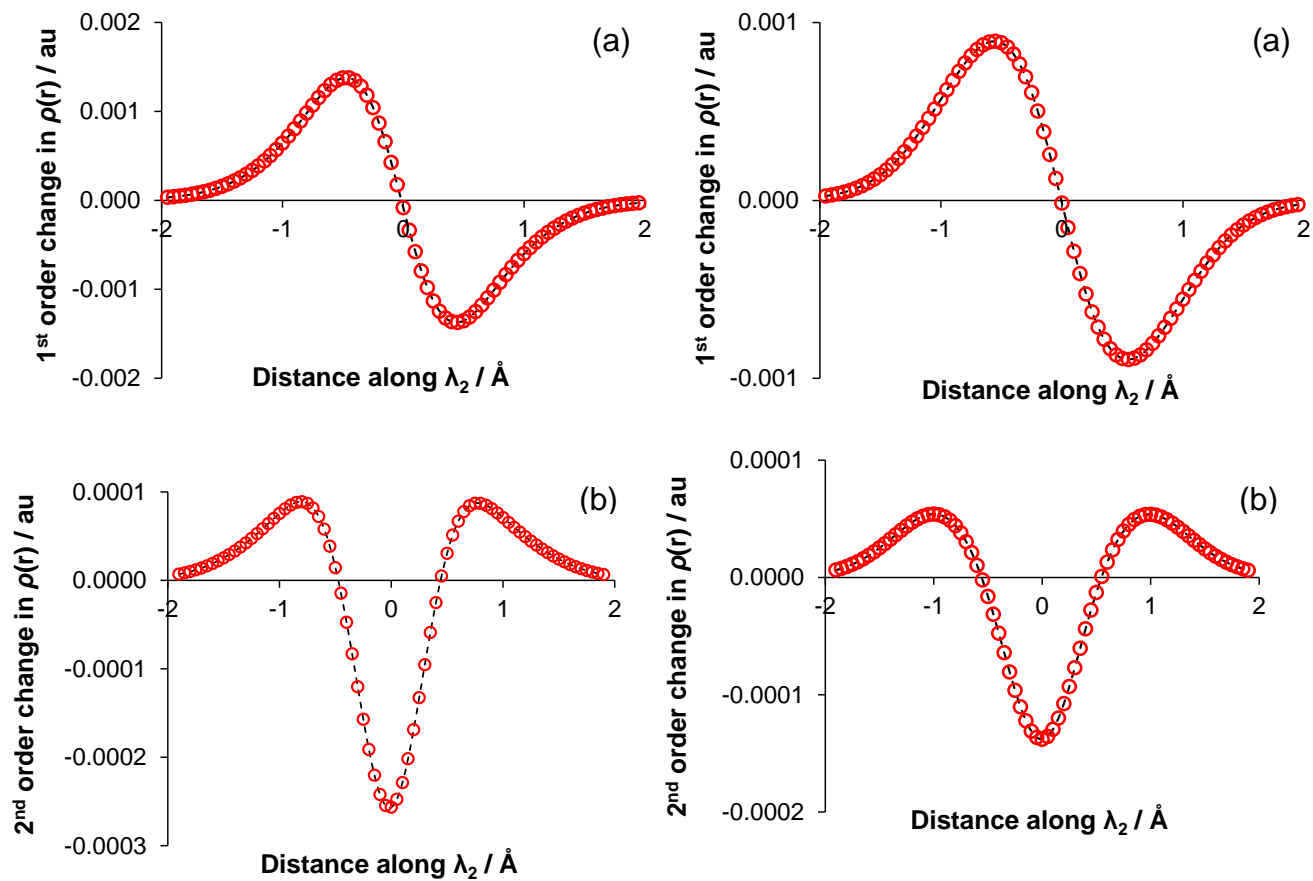


**Figure S8.** Cross sections of the a) 1<sup>st</sup> order and b) 2<sup>nd</sup> order changes in the electron density along the  $\lambda_2$  eigenvector for  $d1$  at  $d(O-H) = 1.946$  Å and  $d2$  at  $d(O-O) = 2.6$  Å. The origin of the cross-sections for  $d1$  and  $d2$  are the BCP(O1,H5) and BCP(O1,O4), respectively.

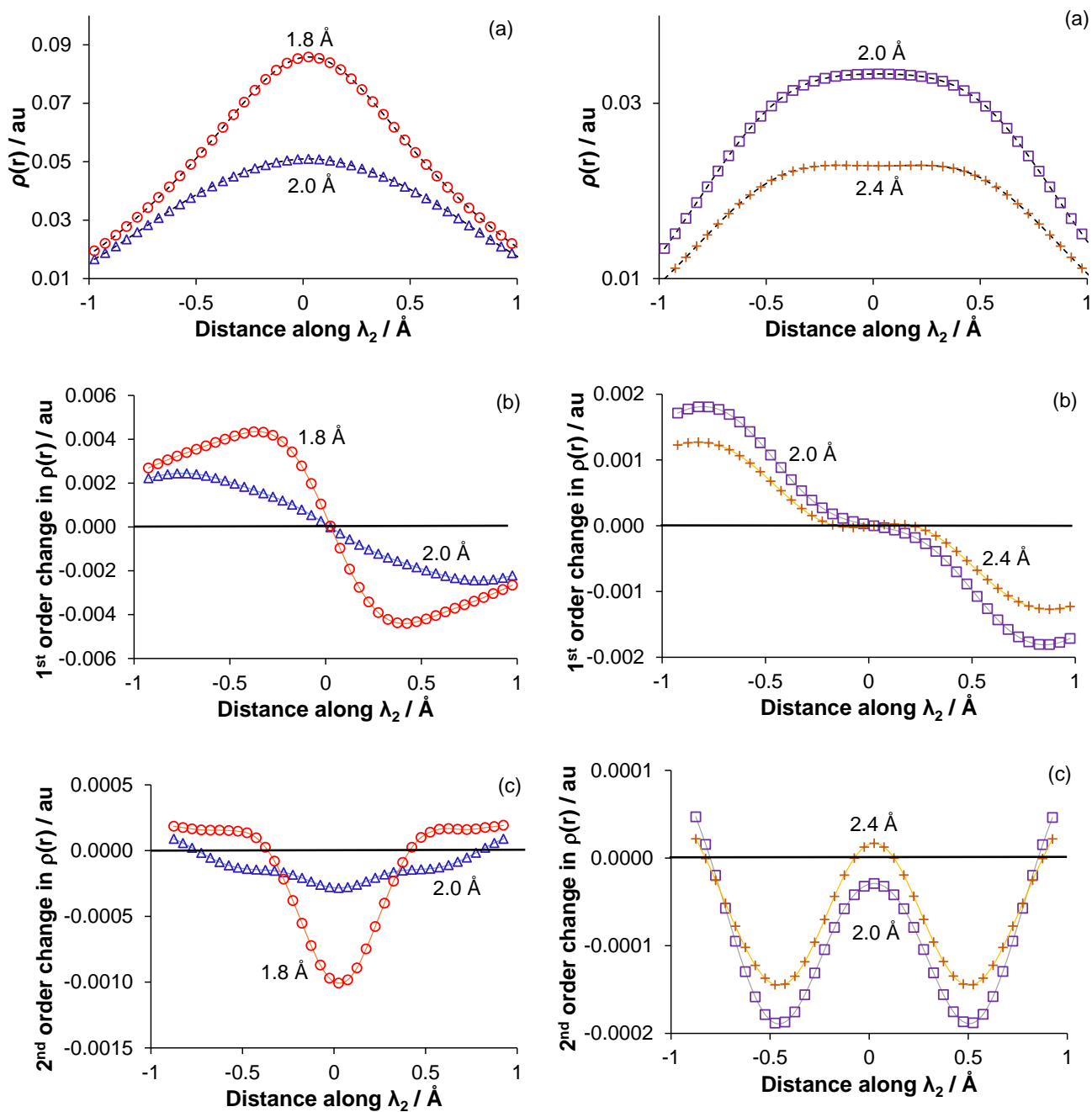


**Figure S9.** Cross-sections of the a) electron density, b) first order and c) second order changes in the electron density of the *d3* water dimer at indicated d(O--O).

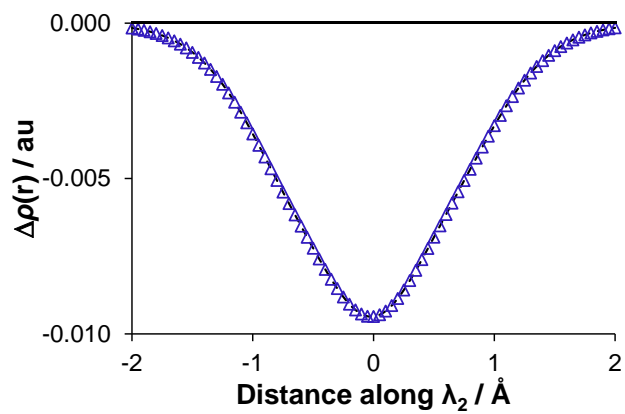


**Figure S10.** Cross-section of the deformation density of the *d3* water dimer at  $d(\text{O}--\text{O}) = 2.0 \text{ \AA}$ .



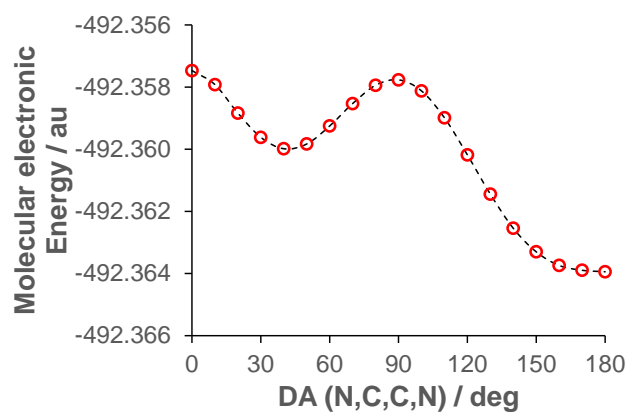


**Figure S11.** Molecular electronic energy, at HF/6-311++G(d,p)/PCM-UFF level, for the rotation of DA(N1,C12,C11,N2) in unprotonated bipyridine.

**Table S2. Molecular electronic energies of unprotonated and protonated bipyridine for different conformers, relative to DA(N,C,C,N) = 90°**

Form	Conformer	DA(N,C,C,N) <i>deg</i>	Relative Energies <i>kcal·mol<sup>-1</sup></i>
L	s-cis planar	0	1.4
	s-cis twisted	37.3	-1.7
	Perpendicular	90	
	s-trans planar	180	-2.6
HL	s-cis planar	0	-5.3
	Perpendicular	90	
	s-trans planar	180	-0.8
H2L	s-cis planar	0	5.5
	s-cis twisted	72.9	0.0
	Perpendicular	90	
	s-trans planar	180	3.5

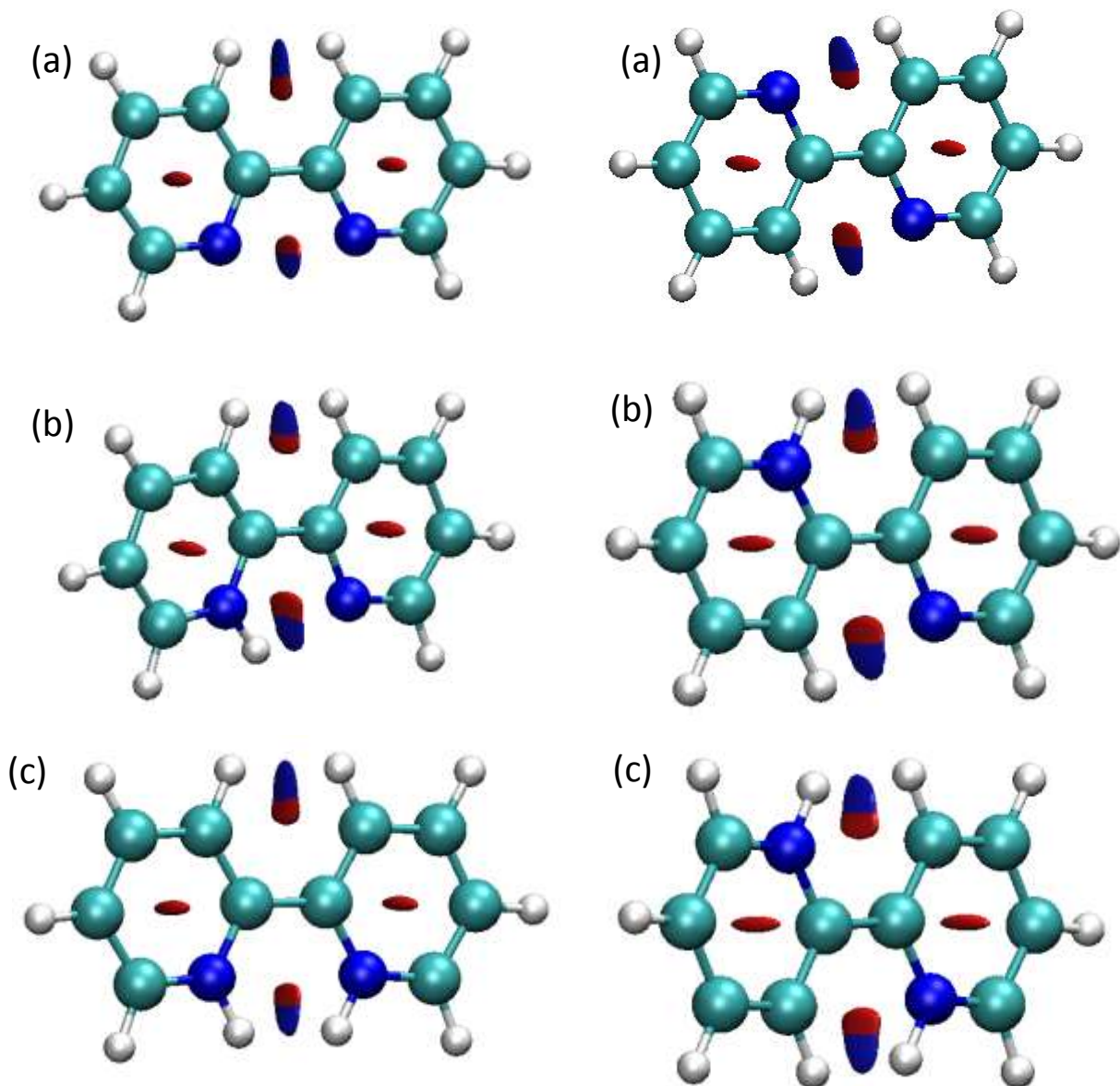


**Figure S12.** NCI isosurfaces of the RDG for the *s-cis* and *s-trans* forms of a) unprotonated bpy, b) protonated bpy and c) diprotonated bpy, with the RDG isovalue = 0.5 au and each isosurface is covered with  $-0.03 \leq \rho \times \text{sign}(\lambda_2) \leq +0.03$  au.

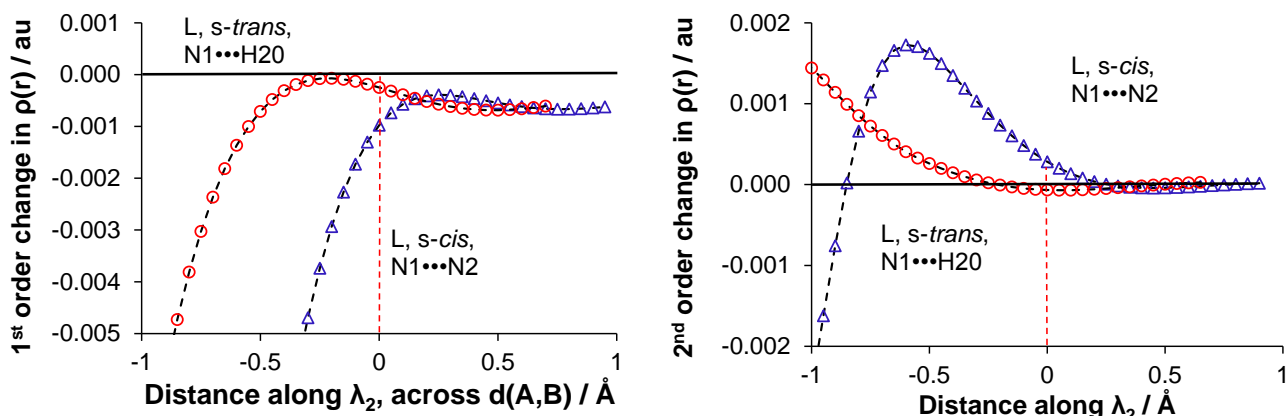


**Figure S13.** Cross-sections of the 1<sup>st</sup> and 2<sup>nd</sup> order changes in the electron density along the  $\lambda_2$  eigenvector of interactions in L, HL and H<sub>2</sub>L bpy without an AIL present. Red dotted lines indicate the geometric interaction point between the nuclei of atoms A and B of each interaction.

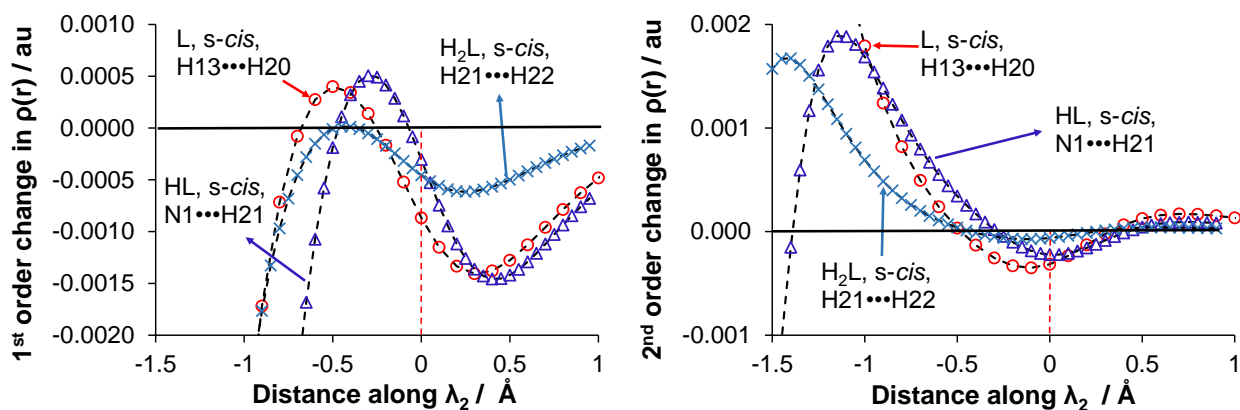


**Figure S14.** Cross-sections of the 1<sup>st</sup> and 2<sup>nd</sup> order changes in the electron density along the  $\lambda_2$  eigenvector of interactions in L, HL and H<sub>2</sub>L bpy with an AIL present. Red dotted lines indicate the geometric interaction point between the nuclei of atoms A and B of each interaction.

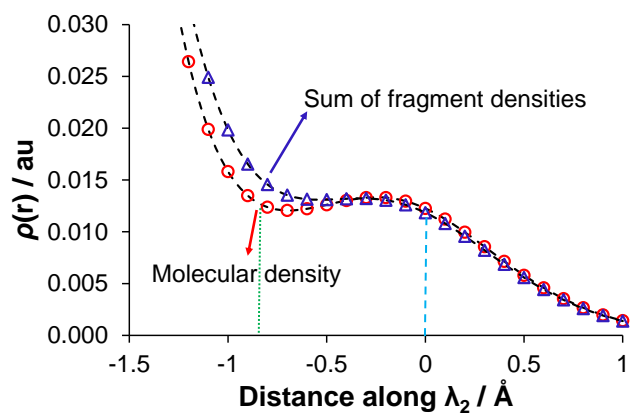


**Figure S15.** Cross-section of the molecular density,  $\rho(\mathbf{r})$ , and the sum of fragment densities,  $\Sigma\rho^0$ , along the  $\lambda_2$  eigenvector for the CH13 $\cdots$ H20C interaction in *s-cis* bpy. The dashed blue line indicates the location of the geometric interaction point, GIP, for the H $\cdots$ H interaction, whereas the dotted green line shows the location of GIP between C-atoms.